COUNTER-PROPAGATING INTRACAVITY OPTICAL TWEEZERS

by

Aysu Ay

B.S., Physics, Boğaziçi University, 2021

Submitted to the Institute for Graduate Studies in
Science and Engineering in partial fulfillment of
the requirements for the degree of
Master of Science

Graduate Program in Physics

Boğaziçi University

2023

ACKNOWLEDGEMENTS

I am thankful for my family who have supported me throughout my education. I believe that my journey so far has provided me with a strong foundation of knowledge and a way of thinking that will guide me in making life decisions. Therefore, I would like to extend my thanks to all my teachers and professors as well, especially Prof. Dr. Mehmet Burçin Ünlü, Dr. Uğur Parlatan, and my thesis supervisor Assist. Prof. Dr. Parviz Elahi. I am truly thankful for the opportunity to pursue such a prestigious course of study. In addition, I would like to express my gratitude to SPIE for student conference support. It provided me with a wonderful experience in Prague where I had the opportunity to interact with worldwide researchers and present my work to them. Moreover, I would like to acknowledge Boğaziçi University Research Fund (Grant number: BAP-21B03SUP3) for supporting this work. It allowed me to establish an entirely new laboratory within our university, leading to my first academic publications and opening the doors for exciting future work.

I am thankful for my sister Melis Ağcaoğlu. Her friendship and existence in my life gives me strength. I am thankful for Dr. Fulya Halıcılar, Dr. Nazik Öğretmen, Dr. İlayda Şahin. They have been constant support, inspiration, and empowerment. I am thankful for Michelangelo Federico. Our endless nights of dreaming for a wonderful future and studying has kept me motivated especially during difficult times. I am thankful for Ali Şen. His love and patience have given me the power to overcome any obstacles in my way. He also has shared with me the wonders of climbing in which he taught me resilience and the ability to navigate difficult situations. I will cherish this beautiful gift for the rest of my life.

I am thankful for that I have accomplished all this hard work during the time of several unfortunate medical issues. Lastly but not least, I am thankful for all Boğaziçi University members who have stood up against discrimination, injustice, and violence.

ABSTRACT

COUNTER-PROPAGATING INTRACAVITY OPTICAL TWEEZERS

Optical tweezers are a powerful tool that utilizes optical forces generated by the exchange of momentum between light and matter to trap and manipulate a wide range of particles, including atoms and molecules, organelles, proteins,and cells.

Since intracavity optical trapping was introduced, a new research opportunity opened for three-dimensional optical trapping of microscopic objects using a low numerical aperture lens at low laser intensity. This method has introduced the placing of the trapping optics within a fiber laser ring cavity and the forces of optical feedback radiation. There are two possible configurations for intracavity optical trapping: single-beam and counter-propagating beam configurations. The former has already been proposed and implemented, while the latter still needs to be discussed in detail: the focus of this work lies on counter-propagating beam configuration.

This work demonstrates the design, implementation, and experimentation of counter-propagating optical tweezers. It presents 3D trapping of 1.98 µm-diameter polystyrene particles, which single-beam intracavity traps were incapable of performing. The total average power on the sample was measured to be 885 µW, which corresponds to an average intensity of 21.2 µW µm^{-2}.

The inversely correlated counter-propagating beams reduce the average intensity on the particle in the trap; hence, they enable the trapping of light-sensitive biological matter. This paves the way for new and exciting applications for optical tweezers.

ÖZET

ÇİFT KİRİŞ KOVUK İÇİ OPTİK CIMBIZLAMA

Optik cımbız, ışık ve madde arasındaki momentum alışverişi tarafından üretilen optik kuvvetleri kullanarak atom ve moleküller, organeller, proteinler, ve hücreler dahil olmak üzere çok çeşitli sayıda parçaçığı tuzağa düşürmek ve manipüle etmek için kullanılan güçlü bir araç olmuştur.

Kovuk-içi optik tuzaklama tanıtıldığından beri mikroskopik nesnelerin düşük sayısal açıklı lens kulllanırak düşük ışık şiddetinde üç boyult tuzaklanması için yeni araştırma fırsatları oluşmuştur. Optik yakalama optik elemanlarını bir fiber kovuk-içine konulmasını ve optik geribildirim radyasyon kuvvelerini tanışmıştır. İki farklı konfigürasyonu vardır: tek ışın ve çift kiriş ışın konfigürasyonları. İlki zaten önerilmiş ve uygulanmıştır, bu çalışmanın odağı ikinci konfigürasyondur.

Bu çalışma, çift kiriş kovuk içi optik cımbızların tasarımını, uygulanmasını ve deneylerini göstermektedir. Tek ışın kavuk içi optik cımbızlarının yakalayamadığı 1.98 µm-çaplı polistiren parçacıklarının üç boyutlu yakalanması sunulmuştur. Parçaçık üstündeki toplam ortalama ışık gücü 885 µW olarak ölçülmekte, bu da $21.2\,\mu W\,\mu m^{-2}$. in ortalama ışık yoğunluğuna karşılık gelmektedir.

Ters korelasyonlu çift kiriş ışınlar, tuzaktaki parçacığın üstündeki ortalama ışık şiddetini azaltmaktadır; böylece ışığa duyarlı biyolojik maddelerin tuzaklanmasına olanak sağlamaktadır. Bu optik cımbızlar için yeni ve heyecan verici uygulamaların önünü açmaktadır.

TABLE OF CONTENTS

ACKNOWLEDGEMENTS . . . iii
ABSTRACT . . . iv
ÖZET . . . v
LIST OF FIGURES . . . viii
LIST OF SYMBOLS . . . xi
LIST OF ACRONYMS/ABBREVIATIONS . . . xiv
1. INTRODUCTION . . . 1
1.1. Historical Background . . . 2
1.2. Applications . . . 5
1.3. Research Motivation . . . 5
1.4. Objectives . . . 6
2. BACKGROUND . . . 7
2.1. Optical Tweezers . . . 7
2.1.1. Optical Setup . . . 8
2.1.2. Optical Trapping . . . 9
2.1.3. Optical Trapping Theory . . . 12
2.1.4. Limitations of Standard Optical Tweezers . . . 14
2.2. Fiber Lasers . . . 15
2.2.1. Continuous-Wave Fiber Lasers . . . 15
2.2.2. Yb-Doped Fiber Laser . . . 17
2.2.3. Yb-Doped Fiber Laser Theory . . . 18
2.3. Intracavity Optical Tweezers . . . 20
2.3.1. Trapping Mechanism . . . 21
2.3.2. Toy Model . . . 22
2.3.3. Limitation of Single-Beam Intracavity Optical Tweezers . . . 24
3. METHODS . . . 25
3.1. CW Fiber Laser Development . . . 26
3.2. Development of Optical Tweezers . . . 27

3.3. Inverted Microscope Assemble 29
3.4. Alignment of The Setup 31
3.5. Sample Manipulation 33
3.6. Data Acquisition 33
3.7. Experiment 35
4. RESULTS 39
4.1. Trapping of Polystyrene Particles 39
4.2. Tracking 40
4.3. Comparison of Optical Tweezers 41
4.4. Limitations of Counter-Propagating Intracavity Optical Tweezers . . . 42
5. CONCLUSION 44
5.1. Findings 44
5.2. Contribution and Significance 45
5.3. Future Work 45
REFERENCES 48

LIST OF FIGURES

Figure 2.1. (a) The schematic of the experimental setup of a single-beam optical trapping system. (b) The schematic of the experimental setup of a dual-beam optical trapping system. 11

Figure 2.2. The schematic of the experimental setup of a mirror trapping system [41]. The yellow dashed line shows a closer look at the focus of two beams. 12

Figure 2.3. Scheme of a ring cavity. The pump and signal are depicted in green and red arrows, respectively. Backward pumping on the left (counter-propagating beams) and forward pumping on the right. The isolator ensures the unidirectional propagation of the laser light in the cavity. 16

Figure 2.4. Typical absorption and stimulated emission cross sections of Yb^{3+} [43]. Note that there is a peak of absorption at 976 nm (A), a peak of emission at 1030 nm (B), and the absorption cross section around 1030 nm is very low (C). 17

Figure 2.5. General Yb^{3+} energy level diagram showing various transitions [43]. The ones exploited it this work are highlighted in yellow. Namely, the pump at 976 nm and the signal at 1030 nm. 18

Figure 2.6. Intracavity optical trapping mechanism. The graphs show the scaling curve of the laser (red line) and lasing (blue x) at a given pump power (green dotted line) when (a) there is no particle in the trap (the laser works above threshold (b) when the particle is in the focal spot (the scaling curve shifts right) (c) when the particle moves within the trap (the scaling curve approaches left). 21

Figure 3.1. Schematic setup of counter-propagating intracavity optical tweezers. Red lines show the counter-propagating beams. Yellow lines show the illumination. The green and red arrow shows the direction of the pump and signal beam. 25

Figure 3.2. CW fiber laser development with a single-mode diode pump laser operating at 976 nm. Fibers are taped on a plastic plate (right). . 26

Figure 3.3. The counter-propagating intracavity optical tweezers setup (left). The sample plane on top of the 3D translation stage (right). . . . 28

Figure 3.4. (a) The inverted microscope setup is coupled to the CIOT setup. The yellow arrows depicts the illumination propagation. (b) A White LED is coupled to a multimode fiber for illumination. (c) The field-of-view of the camera. The yellow circle shows the focal spot. 30

Figure 3.5. The LABVIEW environment for the control of the powermeters. . 35

Figure 3.6. A stationary 1.98 µm diameter polystyrene particle is moved (a) in x-axis and (b) in y-axis at the center of the trap. Powers are measured simultaneously and normalized to the power at the center of the focal point [46]. 36

Figure 3.7. The field of view of the camera in two different instants of time (a) and (b) is shown. The trapped particle is shown in the blue circle, while few freely suspended particles are shown in different colors of circles. Note the trajectory of the free particles: they move more than at least twice the particle size whereas the trapped particle is confined in a much smaller area. 37

Figure 4.1. Simultaneous measurement of signal and pump power on the sample [46]. The yellow dashed line marks the time when the particle is at the equilibrium position within the trap. The particle is below the focal point, it is pushed to the axial position of the trap, then it oscillates in the equilibrium position within the trap. 40

Figure 4.2. The tracking of the particle position in the trap from the recorded video [46]. The pixel position of the particle's center is detected frame by frame and then linked to create the trajectory of the particle within the trap region. 41

Figure 4.3. The radial trapping efficiency of trapping polystyrene particles versus the diameter. Comparison among CIOT, SIOT, and standard high NA optical tweezers. The red triangle marks the result of the experiment that is presented in this thesis. Green circle and blue squares marks the results from [11]. CIOT are able to trap the particles that the SIOT fail to trap. 42

LIST OF SYMBOLS

A_{c}	Ion-doped core area
c	Speed of light in vacuum
D	Diameter of the back aperture of the objective
f	Focal length
F	Restoring force
F_{mirror}	Force exerted on the mirror
F_{x}	Restoring force in the x-direction
F_{y}	Restoring force in the y-direction
F_{z}	Restoring force in the z-direction
$\mathbf{F}_{\mathrm{ray}}$	Total force of the rays
F_{g}	Gradient force
F_{s}	Scattering force
${}^3F_{5/2}$	Stark level of the excited state
${}^2F_{7/2}$	Stark level of the ground state
g	Effective gain of the cavity
G_{net}	Net gain
h	Plank's constant
k_{B}	Boltzmann's constant
k_{trap}	Trap stiffness of the trap
l	Loss of the cavity
l_0	Normalization factor for the loss of the cavity
n	A finite number
n_{i}	Refractive index of the medium of incident rays
n_{m}	Refractive index of the surrounding medium
n_{t}	Refractive index of the medium of transmitted rays
N	Population of the excited state
N_0	Population of the excited state determined by the pump power
N_1	Population of the ground state for Stark level ${}^2F_{7/2}$

N_2	Population of the excited state for Stark level ${}^3F_{5/2}$
N_{D}	Yb doping concentration in m^{-3}
p	Momentum
p_{net}	Total change of momentum per second
P	Power
$\dot{P}$	Rate of change of the power
P_0	Proportionality constant
P_i	Power of the incident rays
P_r	Power of the reflected rays
P_{spon}	Power of the spontaneous emission
P_t	Power of the transmitted rays
r	Particle's position
$\hat{\mathbf{r}}_{\mathrm{i}}$	Unit vector in the direction of the incident rays
$\hat{\mathbf{r}}_{\mathrm{r}}$	Unit vector in the direction of the reflected rays
$\hat{\mathbf{r}}_{\mathrm{t}}$	Unit vector in the direction of the transmitted rays
r_{c}	Scaling of the loss with the particle's position
r_{L}	Particle's position corresponding to the lasing threshold
R	Fresnel's reflection coefficient
T	Fresnel's transmission coefficient
T_{K}	Temperature in Kelvin
U	Trapping potential
W	Spontaneous emission rate
W^{a}	Total absorption rate
W^{e}	Total stimulated emission rate
$W^{\mathrm{a}}_{\mathrm{ASE}}$	Absorption rate of ASE
$W^{\mathrm{e}}_{\mathrm{ASE}}$	Emission rate of ASE
$W_{\mathrm{p}}^{\mathrm{a}}$	Absorption rate of the pump
$W_{\mathrm{p}}^{\mathrm{e}}$	Emission rate of the pump
$W_{\mathrm{s}}^{\mathrm{a}}$	Absorption rate of the signal
$W_{\mathrm{s}}^{\mathrm{e}}$	Emission rate of the signal
w_0	The radius of the beam waist

w_f	The radius of the beam waist at the focus
x_{equ}	Equlibrium position of the trap in the x-axis
y_{equ}	Equlibrium position of the trap in the y-axis
z_{equ}	Equlibrium position of the trap in the z-axis
α	Background losses of the cavity other than absorption
γ	Number of photons per second
Γ	Overlap (or filling) factor
$\Delta\lambda$	Spectral width
θ	Angle of incidence
κ	Optical trap stiffness constant
κ_{x}	Optical trap stiffness in x-axis
κ_{y}	Optical trap stiffness in y-axis
κ_{z}	Optical trap stiffness in z-axis
κ_{p}	Proportionality constant
λ	Wavelength
λ_{ASE}	Wavelength of the ASE
λ_{p}	Wavelength of the pump
λ_{s}	Wavelength of the signal
ν	Optical frequency
ρ	probability density of the particle's position
ρ_0	Normalization factor for probability density
σ_{e}	Emission cross section
σ_{a}	Absorption cross section
σ^2	Variance of the particle's position
τ	Relaxation time
τ_{R}	Cavity round-trip time
ϕ	Angle of refraction

LIST OF ACRONYMS/ABBREVIATIONS

2D	Two Dimensional
3D	Three Dimensional
ASE	Amplified Stimulated Emission
CIOT	Counter-Propagating Intracavity Optical Tweezers
CMOS	Complementary Metal-Oxide Semiconductor
CW	Continuous-Wave
DM	Dichroic Mirror
Er	Erbium
He	Helium
IOT	Intracavity Optical Tweezers
IR	InfraRed
LED	Light Emitting Diode
NA	Numerical Aperture
Nd	Neodymium
Nd:YAG	Neodymium-Doped Yttrium Aluminum Garnet
Ne	Neon
NIR	Near InfraRed
OT	Optical Tweezers
RE	Rare Earth
SIOT	Single-Beam Intracavity Optical Tweezers
SLM	Spatial Light Modulator
WDM	Wavelength Division Multiplexer
Yb	Ytterbium

1. INTRODUCTION

Optical tweezers (OT) are powerful tools that utilize optical forces generated by the exchange of momentum between light and matter in order to trap and manipulate a wide range of particles, including atoms and molecules [1], organelles [2], proteins [3] and cells [4]. Since their discovery [5] in the early 70s, optical tweezers have been used in various applications, including cooling and trapping of neutral atoms [6], manipulating virus and bacteria [7], force measurement in cell biology [8]. However, optical tweezers still face certain limitations. The two primary concerns of optical traps are the scattering force and the light intensity at the focal spot. If the scattering force dominates, the resulting net force on the particle acts in the direction of light propagation, thereby preventing successful trapping. On the other hand, when the laser beam is tightly focused, the high-intensity focal point can induce photodamage due to the heating effect resulting from the interaction between the laser and the sample. These limitations are particularly significant in the field of single-molecule biophysics, where particles are extremely sensitive to light intensity.

Since intracavity optical trapping was first introduced [9] in 2012, these challenges have been partially overcome. This innovation opened new research opportunities for three-dimensional (3D) optical trapping of microscopic objects with a low numerical aperture (NA) lens at low laser intensity. Following that, in 2013, experimental realization of intracavity optical trapping was demonstrated where the trapping optics were placed within a fiber ring cavity [10]. Six years later, in 2019, both optical radiation forces and a toy model to explain these nonlinear forces that arise when the trapped particle and the laser power are coupled, were introduced [11]. Although intracavity optical trapping has already demonstrated its potential, the investigation of a new configuration is needed in order to be able to trap smaller particles. This thesis aims to examine intracavity optical tweezers (IOT) and contribute novel findings to the existing body of knowledge, advancing the field and addressing the limitations of current trapping techniques.

1.1. Historical Background

Johannes Kepler proposed the innovative idea that light has the ability to exert force back in the early seventeenth century. The history of physics and optics established that light has momentum, thus, it can exert radiation pressure on physical objects. However, it was not until Maxwell's groundbreaking theory of electromagnetism in the late nineteen century that it became possible to calculate the pressure exerted by light on a surface. The first experimental verification of radiation pressure force was published by Pyotr Lebedev [12] in 1901, and by Ernest Fox Nichols and Gordon Ferrie Hull [13] in 1903 . Both works succeed in detecting the radiation pressure force acting on macroscopic objects, generated by thermal light sources. However, these forces were very small to have practical use. It was with the advancement in laser technology that it became possible to focus enough optical power onto a small area and thus investigate these forces further.

The idea of stimulated emission, which ignited the advent of laser, was proposed by Albert Einstein [14] in 1917. Over the years many researchers exploited that idea and laid the foundation for the invention of the laser. Gordon Gould [15,16] introduced the term laser at a conference in 1959 in his paper "The LASER: Light Amplification by Stimulated Emission of Radiation". The first discovery of the laser was made by Theodore Maiman [17] in 1960 when he demonstrated it by pumping an active medium of ruby crystal. When ruby was irritated with a high-power flash lamp at a wavelength of 550 nm, chromium ions showed a characteristic energy level transition which allowed for stimulated emission. Soon after the announcement of ruby lasers, a few demonstrations of several different lasers come out, including the Helium-Neon (He-Ne) gas laser by William Bennet and Donald Herriott [16] and the uranium-doped calcium fluoride solid-state laser by Peter Sorokin and Mirek Setevenson [18]. Shortly thereafter, in 1961, Elias Snitzer [19] proposed fiber cavities for lasers, called "optical masers" at that time, and laid the foundation for fiber lasers. A few years after that, fiber amplifiers were introduced by Elias Snitzer and Charles Koester [20]. As fiber laser research and development progressed over the years, their capabilities significantly improved.

Advancements in fiber manufacturing techniques allowed for different core geometries, paving the way for several pumping methods. Additionally, the development of doping techniques made it possible to utilize new host materials, including rare-earth ions like ytterbium (Yb), erbium (Er), and neodymium (Nd), enabling a wide range of applications. On top of that, the quality of laser diodes improved, offering emission at wavelengths in the absorption spectrum of rare earth (RE) ions. Passive optical components like isolator, wavelength division multiplexer (WDM), and fiber brag gratings improved too, allowing for better designs and configurations. While the first fiber lasers produced just a few milliwatts of output power, today's fiber lasers can reach power levels as high as 100 kW. Besides power capabilities, fiber lasers are praised for their beam quality. Moreover, the use of optical fibers instead of bulky free-space optics allows for a compact architecture, resulting in easy integration with other systems and applications, including optical tweezers. Furthermore, highly accurate theoretical models of fiber laser have been developed throughout the years. Both numerical and analytical simulations serve as powerful tools to advance the capabilities of fiber lasers. These advancements in laser technology paved the way to further study of radiation forces, enabling scientists to discover practical uses of these forces.

The first observation of acceleration and trapping of freely suspended micron-sized particles by gradient forces of radiation pressure was reported [5] by Arthur Ashkin in 1970. He demonstrated that optical forces can manipulate the position of micron-sized particles in an aqueous medium. Two fundamental forces of radiation pressure were identified: scattering force and gradient force. The scattering force acts in the direction of light propagation, while the gradient force acts in the direction of the intensity gradient of the laser beam. Ashkin managed to successfully trap transparent latex spheres with a high refractive index of 1.56 and a diameter of 2.68 µm. These spheres were suspended in water with a lower refractive index of 1.33, within a 120 µm thick glass cell. The trapping was achieved by employing a pair of counter-propagating argon lasers emitting at a wavelength of 514.5 nm, with a beam waist radius of 6.2 µm, and by using just milliwatts of power. Furthermore, the discovery of stable optical potential wells, in which particles can be trapped in three dimensions, was established. Finally,

it was shown that the acceleration, deceleration, and trapping of microscopic neutral particles were possible by means of mildly focused laser beams. The next advancement in optical trapping was demonstrated [21] by Arthur Ashkin and Joseph Dziedzic the following year, in 1971. In their paper, they presented the levitation trapping of a transparent glass sphere with a high refractive index 1.65 and a diameter of about 20 µm in both air and vacuum. The sphere was levitated by a single vertical continuous-wave (CW) laser emitting at a wavelength of 514.5 nm, with a beam waist of about 25 µm, and a power of 250 mW. In this configuration, the opposing forces of gravity and axial scattering perfectly balanced each other, and the transverse restoring force kept the particle confined within the trap. However, it was proposed that horizontal restoring force is stronger than vertical one, indicating the limitations of 3D trapping. These pioneering works eventually led to the investigation of single-beam gradient force optical traps, today known as optical tweezers. Although it was originally proposed [22] as an atom trap back in 1978 by Ashkin itself, the optical trapping of dielectric particles was experimentally demonstrated [23] for the first time with the infamous paper by Ashkin and his esteemed colleagues Joseph Dziedzic, John Bjorkholm, and Steven Chu in 1986 which paves the way for trapping of macromolecules, colloids, small aerosols and biological matter. The trapping of particles suspended in water of various sizes, from 10 µm to about 25 nm, was reported even smaller sizes were theoretically proposed. In this work, a single laser beam with a wavelength of 514.5 nm was strongly focused to a limiting spot diameter of 0.58 µm. It was the first all-optical single-beam trap which is capable of manipulating particles. In the same year, the trapping of neutral atoms was also reported by Steven Chu and his colleagues [6], for which he shared the Nobel Prize in Physics in 1997 for "development of methods to cool and trap atoms with laser light" [24].

Over the years, there has been an exponential growth in the number of research papers investigating both theoretical and experimental aspects of optical trapping, including photodamage to the trapped particles [25], the effect of polarization [26] and absorption [27] on the efficiency of trapping, and feedback mechanisms [28] to improve trapping. A noteworthy development, which laid the foundation of this thesis, is the

invention of intracavity optical trapping, which was introduced [9] for the first time at a conference in 2012 and widely studied thereafter. This innovative technique introduced and demonstrated a feedback mechanism that decreases the total average power on the trapped particle, which is crucial for the optical trapping of biological matter. In this configuration, the quality factor of a laser cavity is altered by the displacement of the particle such that particle displacement and performance of the laser are coupled. This invention has opened up exciting research opportunities for trapping and manipulating microscopic objects using a low NA lens, resulting in trapping at low intensity.

1.2. Applications

Over the years, the use of optical tweezers expanded into a myriad of interesting applications, revolutionizing various research fields, especially in biophysics. Thanks to Ashkin, optical tweezers have become indispensable in cellular manipulation [29], cellular sorting [30], "internal cell surgery" [31], the study of molecular motors [32] and DNA [33]. Almost half a century after the invention of optical tweezers, Arthur Ashkin was awarded the Nobel Prize in Physics in 2018 for "optical tweezers and their application to biological systems" [34]. Nowadays, optical tweezers technology is continuously bringing innovation to many fields and shows no signs of stopping. Recently, optical tweezers have been adopted in quantum computing by trapping and manipulating ions [35], in space research by characterizing extraterrestrial dust using optical trapping together with Raman spectroscopy [36], and for biosensing applications such as viscosity measurements [37].

1.3. Research Motivation

The number of optical trapping research papers has been constantly growing over the years. Optical tweezers, which did not exist before the invention of lasers, have evolved tremendously over the years, thanks to the development of new techniques and configurations aimed at enhancing their capabilities for a wide range of applications. While optical tweezers have made significant contributions to single-molecule biophysics

and many other fields, certain limitations persist. The main concerns can be expressed through two critical factors: the scattering force and the light intensity at the focal spot. When the scattering force is dominant, the net force on the particle points in the direction of light propagation, making trapping unattainable. Moreover, if the sample is sensitive to light, the interaction between the laser beam and the sample at the high-intensity focal spot can lead to photodamage, restricting the use of optical tweezers in biological systems. Therefore, it is imperative to explore new configurations of optical tweezers that can achieve 3D trapping at even lower laser intensities. In this regard, the previously mentioned intracavity optical trapping method, which utilizes low NA lenses, shows great promise.

1.4. Objectives

Ever since Arthur Ashkin reported the first experimental observation of a single-beam gradient force radiation pressure particle trap, optical tweezers have undergone extensive studies and analyses, leading to significant improvements and finding countless applications across various fields over the years. Currently, the research in the field of optical traps is far from complete. The scientist are still trying to overcome the current limitations of these tools and explore novel applications. Building upon these considerations, this thesis aims to analyze and evaluate optical trapping techniques, focusing on intracavity optical trapping and discuss further capabilities of optical tweezers. The author's intent is to introduce a new experimental configuration that is capable of 3D trapping of smaller particles compared to existing intracavity optical tweezers configurations. This thesis will investigate the forces in play and finally present the author's insights and findings. In addition, the author aims to introduce two different imaging modalities that have been developed alongside this innovative configuration, known as counter-propagating intracavity optical tweezers (CIOT).

2. BACKGROUND

In this chapter, a comprehensive review of optical tweezers, fiber laser basics, and intracavity optical trapping is presented, focusing on the relevant aspects for understanding counter-propagating intracavity optical tweezers, which is the central topic of this thesis.

Firstly, the chapter provides an explanation of the fundamental concepts and theoretical background behind optical trapping, including main methods, key characteristics, advantages, and drawbacks. Secondly, it gives a quick review of fiber lasers, with particular attention on the type required for the counter-propagating intracavity optical tweezers. Lastly, it gives a brief introduction to the theory of intracavity optical trapping and reviews a former experimental configuration that this work aims to improve.

2.1. Optical Tweezers

An overall analysis of optical tweezers from a broad perspective will be presented here. The study of standard optical tweezers setups, a brief introduction to the main methods employed for optical trapping, and a comprehensive theoretical background based on geometrical optics are included.

Optical tweezers use forces of radiation pressure to trap particles near the focal spot and manipulate the dynamics of micro and nanoparticles. The scattering forces push the particle away from the focal spot, whereas the gradient forces, also known as the restoring forces, pull the particle towards the focal spot. When a laser beam is focused, an optical potential well is created. This attracts particles whose refractive index is higher than the surrounding medium towards the focal spot, around where it will be trapped. There exists an equilibrium position of the trapped particle within the trap. Any displacement of the trapped particle away from this point results in a

restoring force that pulls back the particle to the trap region. By good approximation, one can claim that this restoring force is proportional to the displacement of the particle along each direction. It can be described by Hooke's law [38]

$$\begin{cases} F_{\mathrm{x}} \approx -\kappa_{\mathrm{x}}(x - x_{\mathrm{eq}}) \\ F_{\mathrm{y}} \approx -\kappa_{\mathrm{y}}(y - y_{\mathrm{eq}}) \\ F_{\mathrm{z}} \approx -\kappa_{\mathrm{z}}(z - z_{\mathrm{eq}}) \end{cases}, \tag{2.1}$$

where $[x, y, z]$ is the particle's position, $[x_{\mathrm{eq}}, y_{\mathrm{eq}}, z_{\mathrm{eq}}]$ is the equilibrium position of the trap, $[F_{\mathrm{x}}, F_{\mathrm{y}}, F_{\mathrm{z}}]$ is the restoring forces and $[\kappa_{\mathrm{x}}, \kappa_{\mathrm{y}}, \kappa_{\mathrm{z}}]$ is the optical trap stiffness constants in the respective directions. These forces need to be bigger than the scattering forces to achieve trapping. In addition, these forces needs to dominate Brownian motion to keep the particle in the trap and prevent it from diffusing out. A high NA objective lens focuses the laser beam on a tight spot, providing strong gradient forces to trap a particle. In standard optical tweezers, the laser performance is independent of the displacement of the trapped particle.

2.1.1. Optical Setup

Standard optical tweezers consist of a single beam, typically Gaussian, which is strongly focused by an objective with a high NA on a particle whose refractive index is higher than that of the surrounding medium. To achieve adequate trapping, it is crucial to choose an appropriate laser. Depending on the application, significant parameters such as lasing wavelength, output power, beam shape, pointing stability, and polarization must be considered.

Askin's early experiments utilized argon lasers or neodymium-doped yttrium aluminum garnet (Nd:YAG) lasers with wavelengths of 514.5 nm and 1.06 µm, respectively. According to ray approximation [39], wavelength does not contribute to a significant change in optical forces. However, it can be the source of photothermal effects. Near-infrared lasers (NIR) are frequently employed for optical trapping of biological samples to minimize heating effects, thus limiting the likelihood of damaging the sample. The

NIR wavelengths offer a moderately low absorption of water. Regarding laser power, a few hundred milliwatts are more than enough to generate and investigate optical tweezers. Optical trapping is typically achieved with a Gaussian beam in order to take advantage of the symmetry of the trapped microspheres. However, the beam can be modified with a spatial light modulator (SLM) [40] to achieve the trapping of particles with asymmetric shapes. An objective is used for focusing the laser beam. The most important parameter of the objective is the NA, which is computed as

$$\mathrm{NA} = n_{\mathrm{m}} \sin(\theta) = n_{\mathrm{m}} \frac{D}{2f}, \tag{2.2}$$

where n_{m}, θ, D, and f are the refractive index of the surrounding medium, angle of incident, diameter of the back aperture and the focal length of the objective, respectively. If the beam size is smaller than D, Equation (2.2) becomes

$$\mathrm{NA} = \frac{n_{\mathrm{m}}\, w_0}{f}, \tag{2.3}$$

where w_0 is the radius of the beam waist. Note that the laser beam should overfill the objective back aperture to generate a strong optical trap. Objectives with high NA are usually designed to use an immersion medium to optimize the refractive index of the space between the objective and microscope slide (glass). It minimizes refraction which causes the beam to shift in the lateral direction, and also it decreases the losses which gives a better image. Note that water-immersion objectives offer less spherical aberration than oil-immersion objectives, hence offering less decrease in the intensity gradient and more stiffness of the optical trap.

2.1.2. Optical Trapping

Here the main methods for optical trapping, namely single-beam optical trapping, dual-beam optical trapping, and mirror trapping are introduced by explaining their trapping mechanisms, presenting their schematic setups, and highlighting both their advantages and limitations.

Single-beam optical trapping, also known as single-beam gradient force optical trapping [23], adopts the forces that arise when a strongly focused laser beam interacts

with a particle that has a higher refractive index than the surrounding medium. The trapping scheme, which is depicted in Figure 2.1 (a), includes a laser beam, a high NA objective, and a telescope consisting of two lenses. The laser beam is expanded and collimated to fill the back aperture of the objective. Then, it is tightly focused to a diffraction-limited spot which creates a strong optical potential. The particle is intensely pulled toward the focal spot. Once in the spot, the restoring force keeps the particle in the trap. High trapping forces can be achieved, allowing not only the manipulation of microparticles position, but also to measurement of mechanical properties of biological samples. However, scattering forces and the high-intensity focal spot limit the capabilities of single-beam optical trapping. This method suffers from the strong scattering forces which push the particle out of the trap, in the direction of the beam propagation. It has limited control over trapping in three dimensions. Moreover, the high intensity focal spot can cause photodamage and make the trapping of photosensitive samples challenging.

Dual-beam optical trapping, also known as counter-propagating trapping, utilizes the forces generated by two counter-propagating laser beams to trap particles. The trapping scheme, which is depicted in Figure 2.1 (b), consists of two laser sources with equal Gaussian beams and lenses. They are directed in opposite directions, focused, and aligned such that they coincide where they are diverging. The particle is placed in the middle of the beams, where the trapping occurs. This configuration allows for using a low NA lens, resulting in a high field of view and a long working distance. The gradient force of each beam attracts the particle toward the focal spot whereas the scattering forces from the two beams, in the direction of their respective propagation, cancel each other. If the two beams are not perfectly aligned in the exact opposite direction, but a little deviated from 180 degrees, it is still possible to attain trapping. Dual-beam optical trapping has higher stability and efficiency in 3D trapping compared to standard single-beam traps. The stability of the trapping depends on the refractive indices of the particle and the surrounding medium, and the size of the particle as in single-beam optical trapping. Thus, the trapping of particles with low refractive index or that of very small particles becomes challenging. Moreover, the presence of two

laser beams makes the particle more susceptible to photodamage. This approach for balancing scattering forces was initially proposed [5] by Ashkin, but the gradient forces were not identified yet by him at that time. Since then, more modern versions have been developed, and this configuration has also been realized with fiber lasers.

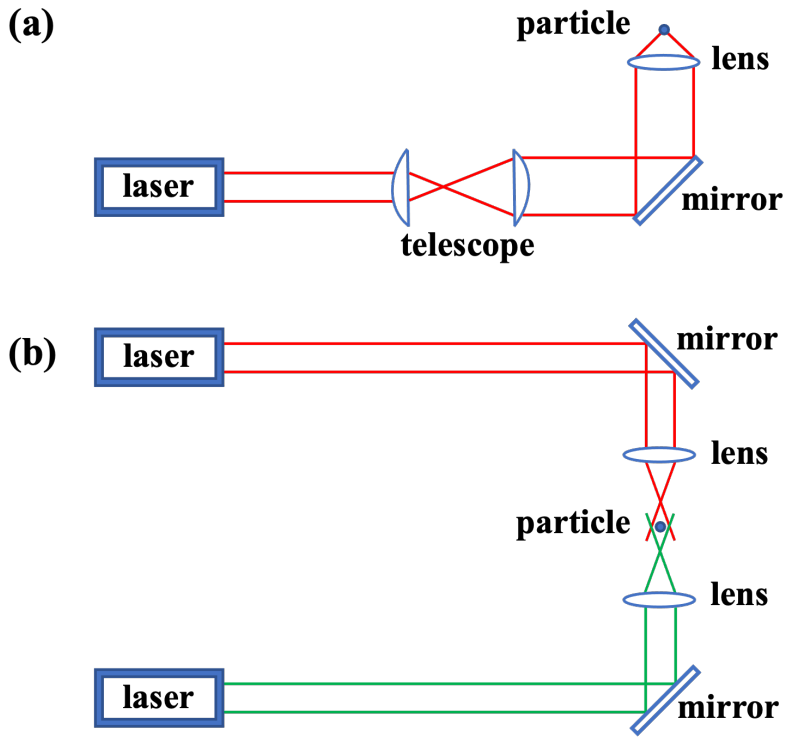

Figure 2.1. (a) The schematic of the experimental setup of a single-beam optical trapping system. (b) The schematic of the experimental setup of a dual-beam optical trapping system.

Mirror trapping [41] is a fairly new method that combines the principles of dual-beam optical trapping and holographic trapping. The trapping scheme, which is depicted in Figure 2.2, is made up of a laser beam, an SLM, a telescope built up by two lenses, a dichroic mirror, and an objective with very low NA. The incoming beam is shaped by the SLM which creates multiple trapping beams with predetermined focus positions. Both beams get focused by the objective with low NA, one is focused before the dichroic mirror, and one is focused after the reflection at the dichroic mirror. The trapping is achieved by gradient forces in the radial direction and scattering forces of both beams in the axial direction. In the case of axial trapping, if the two focal points

perfectly coincide, the scattering forces between two trapping beams cancel each other and the axial component of the gradient force is not enough for 3D trapping. However, if the focal points of the beams are separated by a distance in such a way that the trap center remains at the same position, the mirror trap can tune the stiffness at the center of the trap. This configuration allows for tuning the axial trap stiffness, taking advantage of the low NA lens.

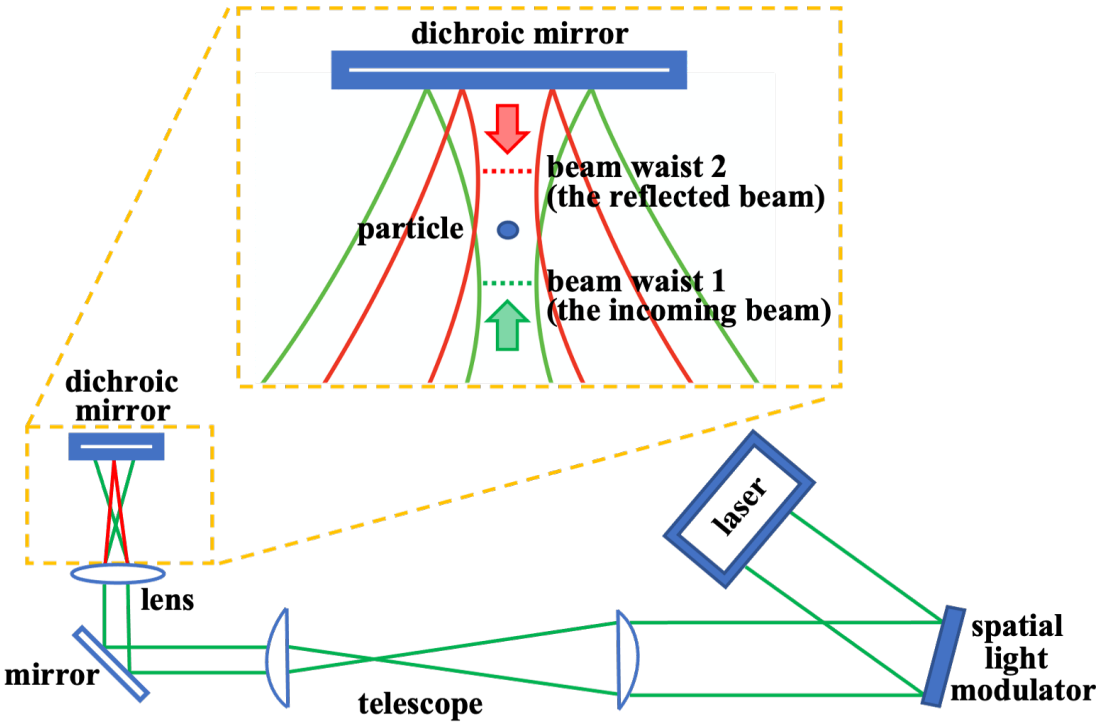

Figure 2.2. The schematic of the experimental setup of a mirror trapping system [41]. The yellow dashed line shows a closer look at the focus of two beams.

2.1.3. Optical Trapping Theory

Optical forces have been studied using approximations that depend on the relative size of the particle with respect to the laser. The calculations of the forces exerted by optical tweezers can be simplified with the Rayleigh regime or geometrical optics regime if the particle's size is smaller or bigger than the trapping light wavelength, respectively. However, if the particle's size is comparable to the wavelength of the laser light, the intermediate regime of complete wave-optical modeling is required to explain

light-matter interactions. In this work, a theoretical treatment of geometrical optics is utilized and therefore discussed below.

The history of optics and electromagnetic theory showed that light carries momentum and it can transfer this momentum to objects, hence can exert force on them. Consider an incident light ray with power P and momentum p carrying γ photons per second, if this hits a reflecting mirror at a right angle, the total momentum change of the light per second is [42]

$$p_{\text{net}} = \left(\frac{2P}{h\,\nu}\right)\left(\frac{h\,\nu}{c}\right) = \frac{2P}{c}, \tag{2.4}$$

where h, ν and c are Planck's constant, frequency of the light, and the speed of light in vacuum, respectively. By the conservation of momentum, this implies that the mirror acquires force with the same magnitude in the direction of light. However, if it is considered that the momentum of a photon increases by a factor n_{m}, the force exerted on the mirror can be written as [38]

$$F_{\text{mirror}} = \frac{n_{\text{m}}\,P}{c}, \tag{2.5}$$

where n is the refractive index of the surrounding medium and F represent the maximum force light can exert at a given power. Suppose a laser beam is focused to a small spot size and it hits a particle, the acceleration of the particle can be easily calculated if it is treated as a reflective mirror.

In geometrical optics, light is considered to be a collection of individual rays where each ray has appropriate intensity, direction, polarization, and characteristic of a plane wave of wavelength equal to zero. These rays are considered to propagate in straight lines in a uniform medium. Each ray can change direction when it reflects and refracts at the surface of the microsphere. Additionally, each ray changes polarization when it interacts with a dielectric interface, following conventional Fresnel formulas. Consider a single ray of power P hitting a dielectric sphere of refractive index higher than the surrounding medium at an angle θ and momentum $\frac{n_{\text{m}}P}{c}$. The net force on the sphere is the vector sum of all forces resulting from reflected rays of power PR and an infinite number of refracted rays of decreasing power P^2TR^n where n is a finite number, R and

T are Fresnel's reflection and transmission coefficients, respectively. The total force on the sphere by the incident, reflected, and refracted rays can be calculated by [38]

$$\mathbf{F}_{\mathrm{ray}} = \frac{n_{\mathrm{i}}\, P_{\mathrm{i}}}{c}\, \hat{\mathbf{r}}_{\mathrm{i}} - \frac{n_{\mathrm{i}}\, P_{\mathrm{r}}}{c}\, \hat{\mathbf{r}}_{\mathrm{r}} - \frac{n_{\mathrm{t}}\, P_{\mathrm{t}}}{c}\, \hat{\mathbf{r}}_{\mathrm{t}}, \tag{2.6}$$

where P_{i}, P_{r},and P_{t} are powers of incident, reflected, and transmitted rays, $\hat{\mathbf{r}}_{\mathrm{i}}$, $\hat{\mathbf{r}}_{\mathrm{r}}$, and $\hat{\mathbf{r}}_{\mathrm{t}}$ are unit vectors in the direction of incident, reflected, and transmitted rays, n_{i} and n_{t} are the refractive index of the medium of the incident rays and transmitted rays, respectively. Using the Fresnel's formulas, the net force on the sphere $\mathbf{F}_{\mathrm{ray}}$ in the Equation 2.6 can be broken down into the scattering component F_{s} and the gradient component F_{g} [39]

$$F_{\mathrm{s}} = \frac{n_{\mathrm{m}}\, P}{c}\left\{1 + R\cos(2\theta) - T^2\, \frac{[\cos(2\theta - 2\phi) + R\cos(2\theta)]}{1 + R^2 + 2R\cos(2\phi)}\right\}, \tag{2.7}$$

$$F_{\mathrm{g}} = \frac{n_{\mathrm{m}}\, P}{c}\left\{1 + R\sin(2\theta) - T^2\, \frac{[\sin(2\theta - 2\phi) + R\sin(2\theta)]}{1 + R^2 + 2R\cos(2\phi)}\right\}, \tag{2.8}$$

where θ and ϕ are angles of incidence and refraction, respectively. This approximation in the calculation of forces can be very useful to explain the mechanism of optical trapping.

2.1.4. Limitations of Standard Optical Tweezers

There are several limitations that optical tweezers have. It was estimated that axial gradient forces are much weaker than the radial ones about the equilibrium point in the trap [21]. The gradient forces in the axial direction need to dominate scattering forces to establish a stable optical potential in which 3D trapping becomes possible. Moreover, standard optical tweezers require a transparent medium in which the particles are suspended to operate efficiently. The presence of an absorbing medium creates significant challenges for trapping. Furthermore, the trap stiffness depends on the size and the refractive index of the trapped particle, and on the power of the laser beam. Small particles with a low refractive index experience weaker trapping forces compared to large particles with a high refractive index. The high intensity of the focal spot generated by a high NA objective can introduce heating effects and photodamage to sensitive biological samples. Thus, it is imperative to investigate new OT configurations

with low NA where 3D trapping at low laser intensity is possible. Intracavity optical trapping, where the particle is trapped within a fiber laser cavity, shows promising results to overcome such limitations mentioned above.

2.2. Fiber Lasers

Fiber lasers are widely used for research thanks to their beam quality, compact size, and robust operation. They are relatively cheap and it is easy to work with them, allowing flexible configurations. They are used in various application, including optical tweezers. They consist of a pump laser in which the active gain medium is an optical fiber commonly doped with rare-earth elements. They convert the input pump radiation energy into a new output source thanks to the active doped-fiber within the resonant cavity. For the sake of relevance to this thesis, only CW fiber lasers with a Yb-doped fiber as a gain medium are reviewed in more detail here.

2.2.1. Continuous-Wave Fiber Lasers

Lasers generate a coherent beam of optical radiation. The three main components of lasers are a pump to supply energy for the excitation of atoms, an active medium to generate optical gain, and a resonant cavity to provide optical feedback to amplify the stimulated emission. A fiber laser is a type of laser that comprises a semiconductor laser for the pump, an optical fiber doped with rare-earth elements for active gain medium, and a cavity mostly made from optical fibers. Doping is adding specific elements into the core of an optical fiber. Depending on the glass composition and doping, the optical properties of the fiber change considerably, making them capable of generating a wide range of different wavelengths of laser light. Passive fibers are mostly made of silica glass in which lasing is not possible. However, when a suitable dopant element is introduced in the core of the fiber, the amplification of stimulated emission becomes possible. Fiber lasers are typically classified as continuous wave or pulsed, and low or high power. CW fiber lasers emit a continuous beam of a laser light as opposed to pulsed lasers that emit short pulses of light. These fibers are pumped

with a continuous light source to excite the doped atoms/ions in doped fiber. The advancement of laser diodes emitting at wavelengths within the absorption spectrum of rare earth ions has led to the common choice of fiber-coupled diode lasers for the pumping of CW fiber lasers.

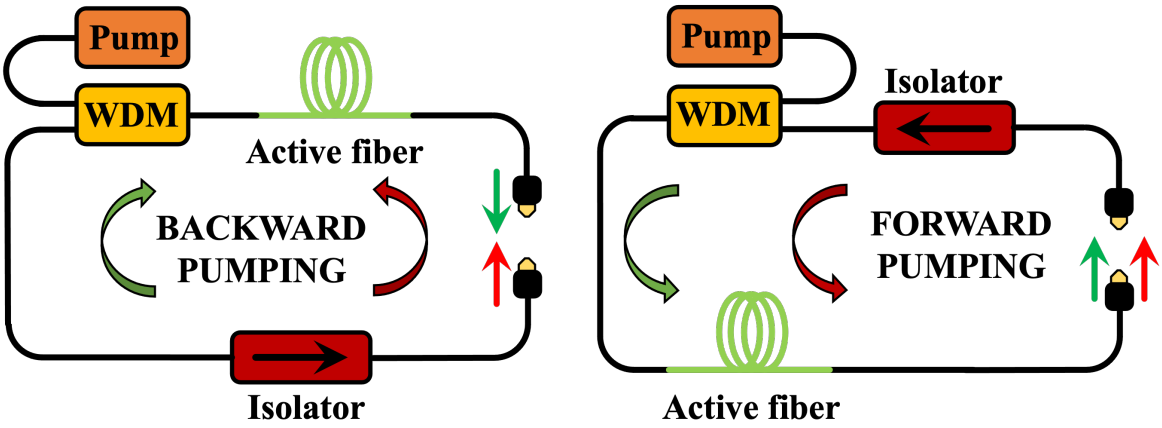

Figure 2.3. Scheme of a ring cavity. The pump and signal are depicted in green and red arrows, respectively. Backward pumping on the left (counter-propagating beams) and forward pumping on the right. The isolator ensures the unidirectional propagation of the laser light in the cavity.

Two main cavity designs could be employed: linear or ring cavity. A linear cavity can be achieved by Fabry-Perot configuration where dichroic mirrors at the end of the optical fiber's faces are employed or by using fiber Bragg gratings. The reflected light provides bidirectional feedback. Ring cavities are used to build intracavity optical tweezers. These can be achieved by creating a loop with passive fibers and optical components. Ring cavity fiber lasers provide the possibility of integrating trapping optics directly inside the cavity, and also allow for low power emissions with stable and narrow linewidth oscillations. The laser light travels in one direction in a ring cavity, either clockwise or counterclockwise. If the cavity is forward pumped, both signal and pump travel counterclockwise, whereas if it is backward pumped, counter-propagating beams are established such that signal light travels counterclockwise and pump light travels clockwise. Figure 2.3 shows both backward (left) and forward (right) pumped ring cavity schemes.

2.2.2. Yb-Doped Fiber Laser

The main mechanisms occurring in the active medium are absorption, spontaneous emission, stimulated emission, and in some cases amplified spontaneous emission (ASE). Figure 2.4 shows the absorption and emission cross-section spectrum of a Yb-doped fiber. These cross-sections are used to quantify the likelihood of both absorption and stimulated emission.

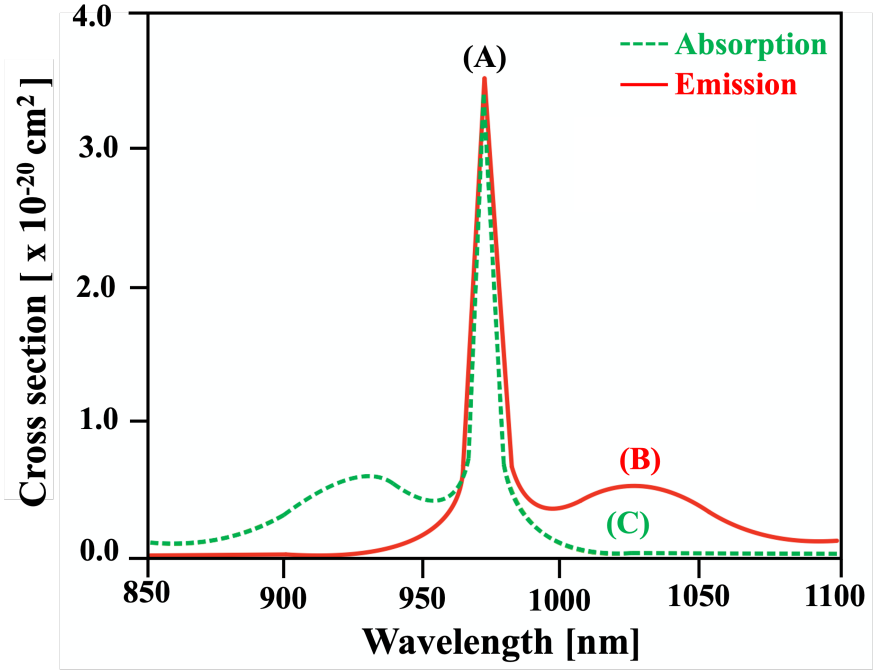

Figure 2.4. Typical absorption and stimulated emission cross sections of Yb^{3+} [43]. Note that there is a peak of absorption at 976 nm (A), a peak of emission at 1030 nm (B), and the absorption cross-section around 1030 nm is very low (C).

Although Yb could be studied as a multi-level system, here it is considered to be a two-level system composed of the stark levels $^2F_{7/2}$ and $^3F_{5/2}$ for the ground and the excited states, respectively. Figure 2.5 shows the energy level diagram of Yb with the most common transitions. When the gain fiber is pumped with the output of a diode laser operating at a wavelength of 976 nm, Yb ions absorb the pump photons energy and get excited to the higher energy state $^3F_{5/2}$ and then slowly decay to the ground state $^2F_{7/2}$ via spontaneous emission by emitting lower energy photons with

a wavelength of 1030 nm. Under high enough pumping power, population inversion can occur. This means that the population of the excited state N_2 is greater than that of the ground state N_1. In this condition, the spontaneously emitted photons at 1030 nm can stimulate the emission of photons with the same phase, wavelength, and polarization by relaxation of the many excited ions.

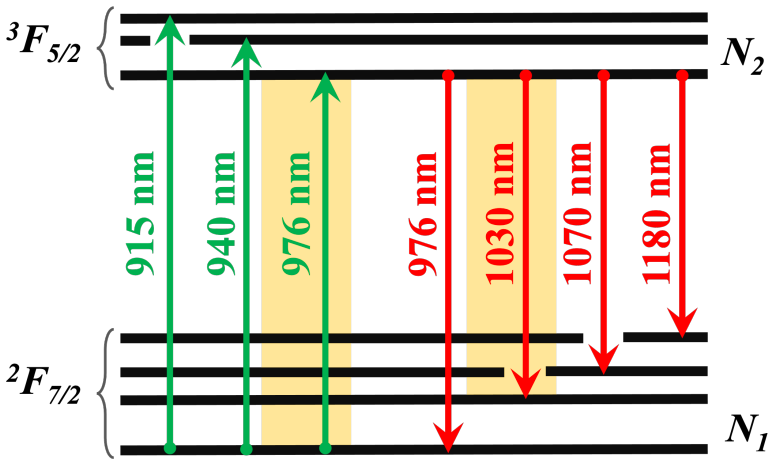

Figure 2.5. General Yb^{3+} energy level diagram showing various transitions [43]. The ones exploited it this work are highlighted in yellow. Namely, the pump at 976 nm and the signal at 1030 nm.

2.2.3. Yb-Doped Fiber Laser Theory

In order to characterize a Yb-doped fiber laser is necessary to have knowledge about the power which is flowing inside the cavity for every position z along the active fiber. In this regard, the power equations for a two-level system are as follows [44]

$$\frac{\mathrm{d}P\left(\lambda_\mathrm{s},z\right)}{\mathrm{d}z} = P\left(\lambda_\mathrm{s},z\right)\cdot\left[g(\lambda_\mathrm{s},z)-\alpha(\lambda_\mathrm{s})\right], \tag{2.9}$$

$$\frac{\mathrm{d}P\left(\lambda_\mathrm{p},z\right)}{\mathrm{d}z} = P\left(\lambda_\mathrm{p},z\right)\cdot\left[g(\lambda_\mathrm{p},z)-\alpha(\lambda_\mathrm{p})\right], \tag{2.10}$$

$$\frac{\mathrm{d}P\left(\lambda_\mathrm{ASE},z\right)}{\mathrm{d}z} = P\left(\lambda_\mathrm{ASE},z\right)\cdot\left[g(\lambda_\mathrm{ASE},z)-\alpha(\lambda_\mathrm{ASE})\right] + P_\mathrm{spon}\left(\lambda_\mathrm{ASE}\right), \tag{2.11}$$

where g is the effective gain, α is the background losses other than absorption, P is power, P_spon accounts for the spontaneous emission into the laser channel, and λ_s, λ_p

and λ_{ASE} are the wavelength of the signal, the pump and the ASE, respectively. Emission and absorption are taken into account by the effective gains of each wavelength λ at position z along the active fiber. The effective gains have all the same expression since only two levels are considered, and can be computed as

$$g\left(\lambda, z\right) = \Gamma\left(\lambda\right)\left[\sigma_{\mathrm{e}}\left(\lambda\right) N_2(z) - \sigma_{\mathrm{a}}\left(\lambda\right) N_1(z)\right], \tag{2.12}$$

where σ_{e} and σ_{a} are the emission and absorption cross sections, N_1 and N_2 the population of the ground and excited states, λ is the wavelength, and Γ is the overlap (or filling) factor, which represents the amount of mode overlap with the doped core. Moreover, for a spectral width of $\Delta\lambda$, the spontaneous emission can be expressed as

$$P_{\mathrm{spon}}(\lambda, z) = 2\,\Gamma(\lambda)\,\sigma_{\mathrm{e}}(\lambda)\,N_2(z)\,\frac{h\,c^2}{\lambda^3}\,\Delta\lambda, \tag{2.13}$$

where h is the Planck's constant and c is the speed of light in vacuum. The dynamics of the populations $N_1(z,t)$ and $N_2(z,t)$ at position z along the Yb-doped gain fiber and time t can then be described by the population rate equations, including terms which represent all the processes that either excite the ions (adding them to the population of the level) or relax them (removing them from the population) [44]

$$\frac{\mathrm{dN}_2(z,t)}{\mathrm{d}t} = N_1(z,t)\;W^{\mathrm{a}} - N_2(z,t)\left(\frac{1}{\tau} + W^{\mathrm{e}}\right), \tag{2.14}$$

$$\frac{\mathrm{d}N_1(z,t)}{\mathrm{d}t} = N_2(z,t)\left(\frac{1}{\tau} + W^{\mathrm{e}}\right) - N_1(z,t)\;W^{\mathrm{a}}, \tag{2.15}$$

where τ is the lifetime of the higher lasing level, $W^{\,\mathrm{a}}$ and W^{e} are the total absorption and stimulated emission rates that can be computed as

$$W^{\mathrm{a}} = \sum_{\lambda} \frac{\Gamma(\lambda)\sigma_{\mathrm{a}}(\lambda)P(\lambda,z,t)}{A_{\mathrm{c}}\cdot h\,c/\lambda}, \tag{2.16}$$

$$W^{\mathrm{e}} = \sum_{\lambda} \frac{\Gamma(\lambda)\sigma_{\mathrm{e}}(\lambda)P(\lambda,z,t)}{A_{\mathrm{c}}\cdot h\,c/\lambda}, \tag{2.17}$$

where A_{c} is the ion-doped core area. The the summations with respect to λ contain the absorption and emission rates of pump ($W_{\mathrm{p}}^{\mathrm{a}}$, $W_{\mathrm{p}}^{\mathrm{e}}$), signal ($W_{\mathrm{s}}^{\mathrm{a}}$, $W_{\mathrm{s}}^{\mathrm{e}}$) and ASE ($W_{\mathrm{ASE}}^{\mathrm{a}}$, $W_{\mathrm{ASE}}^{\mathrm{e}}$). It must be noted that when the pump at 976 nm and signal at 1030 nm are very sharp in wavelength ($\lambda \leq 1\,\mathrm{nm}$), they have one contribution to both summations, while ASE has multiple contributions since it is wide in wavelength ($\simeq 40\,\mathrm{nm}$). Furthermore,

population rate equations can be solved in a steady state regime since the laser is running in CW. By considering that the total Yb concentration must be $N_{\mathrm{D}} = N_1 + N_2$, and solving in steady state regime (derivatives in Equation (2.14) and Equation (2.15) set to zero), the ratio between the population of the excited state with respect to that of the ground state becomes

$$\frac{N_2}{N_1} = \frac{W_{\mathrm{p}}^{\mathrm{a}} + W_{\mathrm{s}}^{\mathrm{a}}}{W_{\mathrm{p}}^{\mathrm{a}} + W_{\mathrm{p}}^{\mathrm{e}} + W_{\mathrm{s}}^{\mathrm{a}} + W_{\mathrm{s}}^{\mathrm{e}} + W_{\mathrm{ASE}}^{\mathrm{e}} + \frac{1}{\tau}}, \tag{2.18}$$

where $W_{\mathrm{ASE}}^{\mathrm{a}}$ is set to zero since the absorption cross section around 1030 nm is very low (point (C) in Figure 2.4). The lasing is possible if and only if population inversion is achieved where N_2 is bigger than N_1.

2.3. Intracavity Optical Tweezers

Intracavity optical tweezers use forces of optical feedback radiation to trap particles inside a fiber laser cavity and to manipulate the dynamics of microparticles. When an intrinsic closed-loop control is established within a laser cavity, intracavity nonlinear feedback forces emerge. This approach reduces the average intensity, hence preventing possible photodamage. It allows to employ a low NA lenses which gives a wide field of view and a long working distance. Feedback mechanisms are widely utilized in optical tweezers to control the particle's position or the trapping force. However, a configuration that exploits a feedback mechanism between the laser beam and the microparticles has not been used until intracavity optical tweezers were introduced. There are two possible configurations for intracavity optical trapping: single-beam and counter-propagating beam configurations. The former has already been proposed and implemented [11]; the focus of this work lies on the latter configuration. The single-beam intravity optical tweezers (SIOT) consist of single-beam inside a CW ring cavity fiber laser, trapping optics that are placed inside the cavity, a sample manipulation system, and an imaging system to monitor the experiment. The laser beam is directed upward, and trapping is realized by an aspheric lens with a focal length of 8 mm. The counter-propagating beam optical tweezers will bu discussed at Chapter 3 where the design, implementation and experimentation will be presented.

2.3.1. Trapping Mechanism

In intracavity optical trapping, the particle is trapped inside the ring cavity of a fiber laser. The displacement of the particle results in a response that affects the laser emission. A change in the laser emission results in a response that affects the displacement of the particle. Figure 2.6 illustrates the trapping mechanism where the laser performance and the particle's position is coupled. When there is no particle in the trap, the optical loss of the cavity is at its minimum. The laser operates above the threshold, generating a strong optical potential, and attracting the particle. When the particle approaches the focal spot, it scatters light outside of the cavity, increasing the cavity loss and reducing the quality factor of the cavity. Thus, when the particle is in the trap, the lasing threshold increases and the laser turns off. Conversely, when the particle is free to escape and moves away from the trap, it scatters less light, decreasing the lasing threshold and increasing the laser power. The particle gets attracted back to the recurrent strong optical potential. This mechanism allows for self-regulation of laser power, enabling trapping with a low NA lens at a low total average intensity. Intracavity nonlinear feedback forces emerge when this feedback mechanism between the particle and laser is implemented, allowing a more efficient optical tweezer.

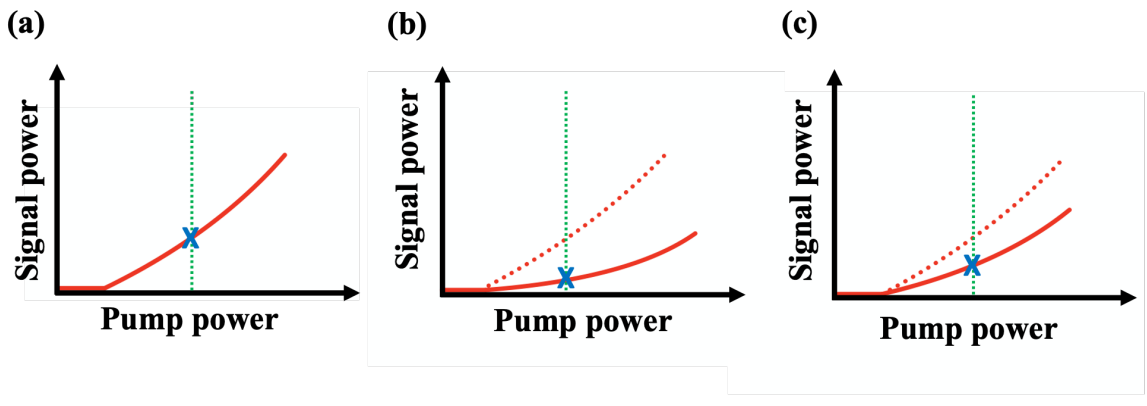

Figure 2.6. Intracavity optical trapping mechanism. The graphs show the scaling curve of the laser (red line) and lasing (blue x) at a given pump power (green dotted line) when (a) there is no particle in the trap (the laser works above threshold (b) when the particle is in the focal spot (the scaling curve shifts right) (c) when the particle moves within the trap (the scaling curve approaches left).

2.3.2. Toy Model

A simple toy model is employed for intracavity optical trapping in order to explain how the nonlinear feedback forces emerge when the dynamics of the particle and the laser are coupled. The analytical methods discussed in detail in [11] will be revived here. The intracavity optical trapping uses a model for laser dynamics where the rate of change of the power, $\dot{P}$, can be computed as [11]

$$\dot{P} = N\,W\,P - \frac{l(r)}{\tau_{\mathrm{R}}}P, \tag{2.19}$$

where N is the electron population in the excited state, W is the spontaneous emission rate at which excited electrons relax to the ground state, P is the power that circulates in the cavity, τ_{R} is the cavity round-trip time, and $l(r)$ is the loss of the cavity, which depends on the particle position r. The electron population in the exited state, N, can be described as [11]

$$N = N_0 - P\,\frac{2N_0\,\tau}{h\,\nu}, \tag{2.20}$$

where N_0 is the population in the excited state determined by the pump power,τ is the relaxation time of the excited electrons, h is the Planck's constant, ν is the optical frequency of the laser output. Inserting N into the Equation (2.19) gives [11]

$$\dot{P} = G_{\mathrm{net}}(r)\,P - \frac{2N_0\,\tau\,W}{h\,\nu}P^2, \tag{2.21}$$

where G_{net} is the net gain which can be computed as [11]

$$G_{\mathrm{net}}(r) = N_0\,W - \frac{l(r)}{\tau_{\mathrm{R}}}, \tag{2.22}$$

which is a function of particle position. The cavity loss is maximum when the particle is at the center of the focal spot as it scatters the greatest amount of laser light. For a small displacement of the particle, cavity loss can be modeled as [11]

$$l(r) = l_0\left(1 - \frac{r^2}{r_{\mathrm{c}}^2}\right), \tag{2.23}$$

where r_{c} characterizes the scaling of the loss with the particle's position and l_0 is a normalization factor for the loss of the cavity. If the lasing threshold condition, which depends on the displacement, is defined as r_{L}, one can say that for a displacement

$r < r_{\mathrm{L}}$ the net gain of the laser is negative, so the laser turns off. If the particle displacement is more than r_{L}, the laser turns on, and the power increases quadratically with r.

The timescale for the particle displacement is in the order of milliseconds, whereas the response time of the laser is in the order of nanoseconds. Thus, it is considered that the laser is always in its steady state regime regarding the coupling with the displacement of the particle. Therefore, the power at the steady state is [11]

$$P(r) = \begin{cases} 0, & \text{if } r \leq r_{\mathrm{L}} \\ P_0 \left(\frac{r^2}{r_{\mathrm{L}}^2} - 1 \right), & \text{if } r > r_{\mathrm{L}} \end{cases}, \tag{2.24}$$

where P_0 is a proportionality constant. The trap stiffness is proportional to the power, hence the displacement of the particle. Using Hooke's law, the restoring force which depends on r can be computed as [11]

$$F(r) = -k\, r = -\kappa_p\, P(r)\, r = \begin{cases} 0, & \text{if } r \leq r_{\mathrm{L}} \\ -P_0\, \kappa_p \left(\frac{r^2}{r_{\mathrm{L}}^2} - 1 \right) r, & \text{if } r > r_{\mathrm{L}} \end{cases}, \tag{2.25}$$

where κ_p is a proportionality constant that depends on the geometrical and optical properties of the setup and the sample but it is independent of the laser power. As opposed to standard optical tweezers, the restoring force is non-harmonic because of its dependence on r. This dependency on r forms the foundation of the nonlinear feedback force. The trapping potential is given by [11]

$$U(r) = -\int_0^r F(x)\, \mathrm{d}x = \begin{cases} 0, & \text{if } r \leq r_{\mathrm{L}} \\ -P_0\, \kappa_p \left(\frac{r^4}{4 r_{\mathrm{L}}^2} - \frac{r^2}{2} + \frac{r_{\mathrm{L}}^2}{4} \right) r, & \text{if } r > r_{\mathrm{L}} \end{cases}, \tag{2.26}$$

in which the probability density, ρ, of the particle position can be determined by the Maxwell-Boltzmann distribution as follows

$$\rho(x) = \rho_0 \exp\left[-\frac{U(x)}{k_{\mathrm{B}}\, T_{\mathrm{K}}} \right], \tag{2.27}$$

where ρ_0, k_B, T_{K} is the normalization factor, the Boltzmann constant and the temperature in Kelvin, respectively. The probability density of particle's position describes the motion of an optically trapped particle. A particle with Brownian motion is in a

dynamic equilibrium where it tries to diffuse away from the trap but the optical forces pull it toward the center of the trap. In intracavity optical trapping, the probability density of the particle's position inside of the trap becomes

$$\rho(r) = -\rho_0 \exp\left[-\frac{U(r)}{k_{\mathrm{B}}\,T_{\mathrm{K}}}\right] = \begin{cases} \rho_0\,, & \text{if } r \le r_{\mathrm{L}} \\ \rho_0 \exp\left[-a\,r^4 + b\,r^2 - \frac{1}{2}b\,r_{\mathrm{L}}^2\right], & \text{if } r > r_{\mathrm{L}} \end{cases}, \quad (2.28)$$

where $a = \frac{P_0\,\kappa_{\mathrm{P}}}{4r_{\mathrm{L}}^2\,k_{\mathrm{B}}\,T_{\mathrm{K}}}$ and $b = \frac{P_0\,\kappa_{\mathrm{P}}}{2k_{\mathrm{B}}\,T_{\mathrm{K}}}$ are constants. With this toy model, one can also solve exactly the expression for the variance of particle position, and the average laser power on the particle exactly. This analytical model describes the optical trapping scheme of single-beam intracavity optical tweezers.

2.3.3. Limitation of Single-Beam Intracavity Optical Tweezers

This configuration suffers from the scattering force toward the laser light. The scattering force pushes the particle along the direction of the laser, thus does not permit to trap a few microns or nanoparticles. It cannot trap polystyrene particles with a diameter smaller than 4 µm.

3. METHODS

This chapter aims to provide detailed explanation of design, implementation, and experimentation of counter-propagating intracavity optical tweezers which promises trapping of smaller particles that the single-beam configuration were unable to achieve.

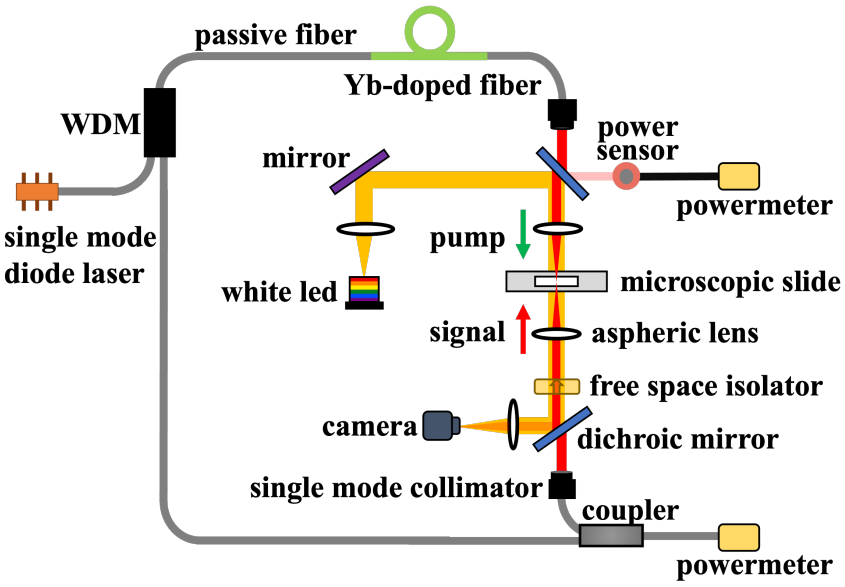

Figure 3.1. Schematic setup of counter-propagating intracavity optical tweezers. Red lines show the counter-propagating beams. Yellow lines show the illumination. The green and red arrow shows the direction of the pump and signal beam.

The counter-propagating optical tweezers configuration consists of two counter-propagating beams and trapping optics inside a CW ring cavity fiber laser, a sample manipulation stage, and a custom inverted microscope. Figure 3.1 depicts the scheme of a CIOT setup. It is crucial to establish mechanical stability in both microscope and optical tweezers. The system is built on an optical table that insulates any environmental vibrations. An optical breadboard is mounted on a vertical optical rail which is set on the optical table. Optical trapping optics are assembled on the rail while an inverted microscope setup is partly mounted on the breadboard. The purpose of using such a configuration is to keep the setup compact and easy to move without compromising its mechanical stability.

3.1. CW Fiber Laser Development

This configuration uses a fiber-coupled diode laser and free space optics to create a CW ring cavity fiber laser with an all polarization-maintaining (PM) fiber operating at a central wavelength of 1030 nm. Figure 3.2 shows the CW laser which consists of a single-mode diode emitting at 976 nm, a segment of Yb-doped fiber as the gain medium, a wavelength division multiplexer to combine the pump at 976 nm and the signal generated by the laser at 1030 nm, a 95%/5% inline coupler, two single-mode fiber pigtailed collimators, and a free space isolator.

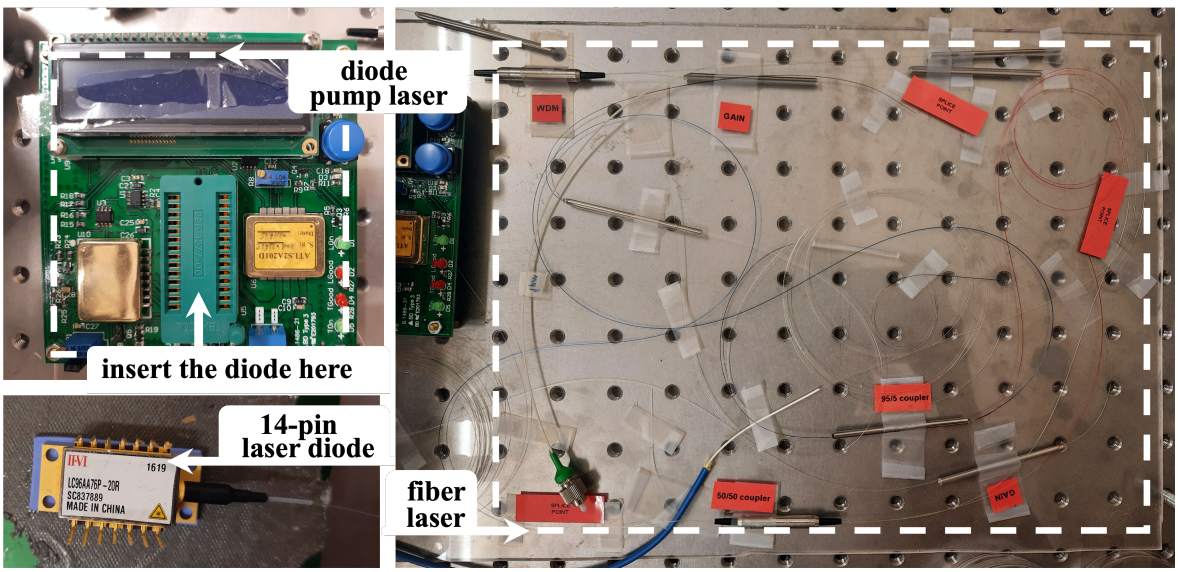

Figure 3.2. CW fiber laser development with a single-mode diode pump laser operating at 976 nm. Fibers are taped on a plastic plate (right).

The pump laser is a 14-pin single-mode, fiber-coupled, wavelength-stabilized diode operating at a wavelength of 976 nm. The bandwidth of the laser is less than 1 nm, and the maximum output power is about 600 mW. The diode is run by a low-noise current source driver which enables the generation of a maximum current of about 1 A. The accuracy of the driver is about 1 mA. The current of the driver is altered to change the power of the laser, however, a half-wave plate and polarizer are recommended for power change to protect the laser beam emission quality. A heat sink is placed on top of the diode to remove the heat that it generates.

The WDM (1030/976 Ligthel Technologies) has 3 ports: a 976 nm port, a 1030 nm port, and a common port to combine both beams. The accuracy of the WDM is about ± 5 nm. The 976 nm port is spliced to the output of the pump laser. The 1030 nm port is spliced to the 95%/5% inline coupler, the smaller portion is used as a monitoring port, and the greater portion is spliced to the bottom collimator. The 5% monitoring port is then connected to another 50%/50% coupler with one PM fiber and one non-PM fiber. One port is used for power, and the other is for polarization monitoring. The common port which combines both beams is spliced to the 40 cm long Yb-doped fiber (Yb-1200, 6/125) which is spliced to the top collimator. Two collimators (6/125, OZ Optics) have been mounted in very precise kinematic mounts. The beam size of the collimator is about 1.4 mm.

The pump at 976 nm travels to the gain fiber through the common port. The unabsorbed pump will travel unidirectionally through the top collimator whereas the emission at gain fiber will travel bi-directionally through the 1030 nm port and the top collimator. A free space polarization-dependent isolator (1060, low power, Thorlabs) is employed to make the signal beam propagate only backward within the cavity, hence a backward pumping fiber laser for trapping is established. It also blocks the backward traveling ASE, which improves the efficiency of the amplifier.

3.2. Development of Optical Tweezers

This configuration uses a CW ring cavity fiber laser and free space optics. In contrast to extracavity optical tweezers, in this case, the trapping optics are also part of the cavity. They are all inserted along a vertical rail to take advantage of gravity. The counter-propagating optical tweezer optics consist of the free space isolator for backward pumping, two lenses to create a focal spot for trapping, collect the scattered light from the sample and send it back into the cavity, and two dichroic mirrors (DM) for illumination propagation. Figure 3.3 shows a closer look at the trapping optics. The free space isolator is employed to allow the laser light to travel in one direction inside the cavity. With the presence of an isolator at its position, the signal beam at 1030 nm

propagates from the bottom to the top whereas the pump beam at 976 nm propagates from top to bottom, hence counter-propagating beams for trapping is established. This configuration utilizes the inversely correlated two counter-propagating beams, the signal beam from bottom to top and the pump from top to bottom. Moreover, the scattering forces in the axial direction are canceled, resulting in stronger trapping strength.

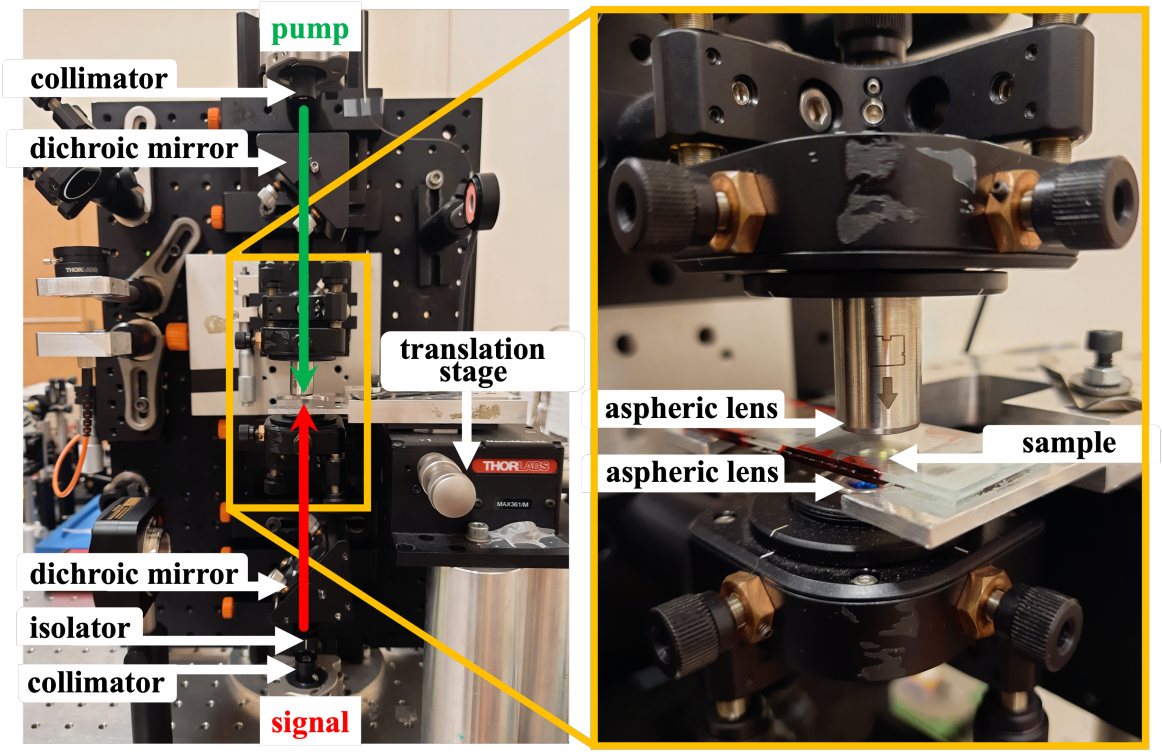

Figure 3.3. The counter-propagating intracavity optical tweezers setup (left). The sample plane on top of the 3D translation stage (right).

The 8 mm focal length aspheric lenses with 0.125 NA are employed to focus the counter-propagating beams on the sample. They are mounted on five-axis kinematic mounts (Thorlabs) for precise alignment. The beam diameter at focus is calculated with the following relation

$$2w_{\mathrm{f}} = \frac{2\lambda f}{\pi w_0}, \tag{3.1}$$

where w_{f} and w_0, are the radius of the beam waist at the focus and at the output of the laser, λ is wavelength, and f is the focal length of the lens. The calculated

beam diameter at the focus is 7.1 µm and 7.5 µm at pump and signal wavelengths, respectively. The novelty of this configuration lies in the ability to use an ultra-low NA lens for trapping of small particles which have a diameter smaller than 2 µm.

The beam from the bottom lens is collected at the top lens and coupled to the top collimator. When the particle is around the focal spot, it scatters light, resulting in cavity loss. The particle's position changes the amount of light that is collected and returned to travel in the cavity, determining the performance of the laser. The optical loss that the particle introduces to the cavity of the laser affects the pump and signal powers. Hence, the feedback between the particle displacement and the laser performance regulates the total average power on the sample.

Lastly, a couple of long pass DMs at 900 nm cut-on are employed for illumination. They transmit and reflect wavelengths longer and shorter than 900 nm, respectively. It allows to image the sample without interfering with the cavity.

3.3. Inverted Microscope Assemble

Integration with an imaging system is necessary for the implementation of any optical tweezers. A homemade inverted microscope in Figure 3.4 (a) is built and for imaging in counter-propagating intracavity optical tweezers.

Bright-field illumination is used where the sample is illuminated by a white high-power light emitting diode (LED), with a maximum output power of 3 W. The white light is transmitted through the sample onto the camera. As shown in Figure 3.4 (b), the LED is coupled to a multimode fiber because of the its divergence. The output of the fiber is mounted on the breadboard to easily couple the illumination with laser beams along the vertical axis of the setup. A 35 mm focal length lens is used to collimate the output diverging light from the fiber. The illumination brightness is adjusted by altering the current in the power source of the LED and altering the aperture of the pinhole that is mounted on the collimating lens. A mirror at 45 degrees is mounted on

the breadboard to reflect the collimated light toward the top DM. The long pass DM at 900 nm cut-on allows to reflect the light and transmit the laser beam toward the upper lens. The trapping optics are also a part of the homemade inverted microscope. The use of a low NA lens allows for a large field of view which is depicted in Figure 3.4 (c). The light is focused on the sample, then the transmitted light is collected with the bottom lens and it is reflected at the bottom DM toward another lens. It is focused on the camera with complementary metal oxide semiconductor (CMOS) sensor (1.3 Megapixel, Thorlabs), which is connected to the computer.

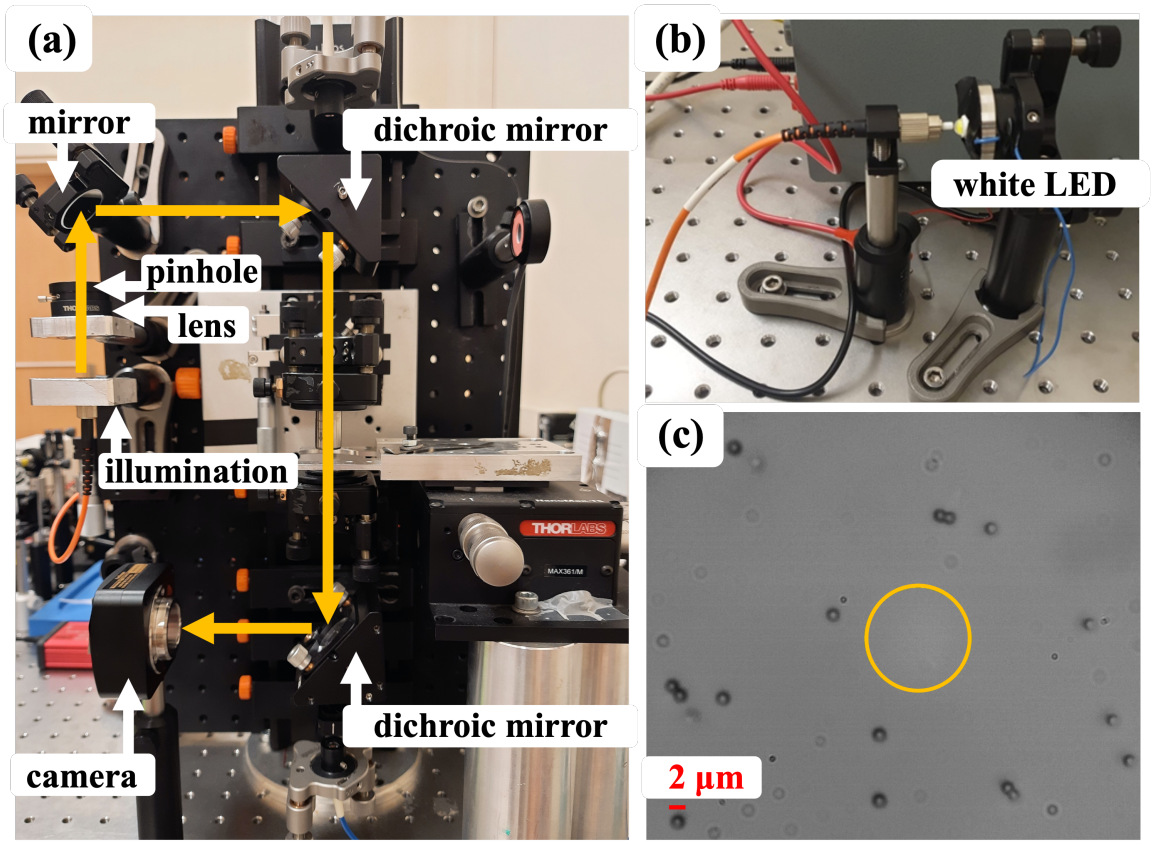

Figure 3.4. (a) The inverted microscope setup is coupled to the CIOT setup. The yellow arrows depicts the illumination propagation. (b) A White LED is coupled to a multimode fiber for illumination. (c) The field-of-view of the camera. The yellow circle shows the focal spot.

The camera is placed on the optical table to have more convenient control over its position, however, it can also be mounted on the breadboard. Alignment of the

camera is crucial for the quality of the image, if not implemented correctly, distortions prohibit having a reliable image of the sample. An aspheric lens with a long focal length before the camera could be used for magnification, however, the amount of light that reaches the camera decreases, consequently decreasing the contrast on the image. The contrast in the image is regulated by a pinhole and a red filter placed on top of the pinhole. A monochrome image is used for more efficient tracking. A short pass filter on the camera is used to remove saturated laser light in the image. While this configuration gives the whereabouts of particles in the axial direction, it is capable of measuring the particle's position only in the radial direction.

3.4. Alignment of The Setup

The setup of the counter-propagating optical tweezers begins with the alignment of the counter-propagating beams in the free-space cavity. The optics are mounted on a vertical rail so that the axial direction of the laser aligns with gravitational acceleration. At first, two collimators are mounted in very precise kinematic mounts with three manual actuators which allow $\pm 4^\circ$ of pitch and yaw adjustment. They are attached to optical rails. The counter-propagating beams from the collimators are finely aligned with each other to establish the feedback in the cavity. The signal power is maximized. After that, the DMs are mounted in right-angle kinematic cage mounts with two manual actuators which allow $\pm 4^\circ$ of pitch and yaw adjustment. The mirrors are placed diagonally between the collimators such that the 976 nm beam from the top and the 1030 nm beam from the bottom pass through and meet in the middle, but the illumination enters and leaves the cavity. They are placed in kinematic mounts, allowing fine control over the propagation of illumination. Around 6-8% cavity loss is observed. The propagation of the reflected beams from the DMs should be checked to ensure they are parallel to the optical table. It will confirm that the pump and signal are perpendicular to the gravitational acceleration. A little manipulation of the DMs actuators will help to achieve the desired propagation. In the next step,the free space polarization-sensitive optical isolator is placed between the bottom collimator and bottom DM for the signal to counter-propagate within the cavity. The polarization is

altered until reaching maximum power. About 60% cavity loss is observed. An inline isolator is recommended to achieve less optical loss. The last step of the alignment of the counter-propagating beams is the placement of the plano-convex lenses with a focal length of 8 mm. It is the most sensitive part of the alignment. Lenses are mounted on five-axis kinematic mounts with five manual actuators which allow $\pm 4^{\circ}$ of pitch and yaw adjustment at 8 miliradian per revolution, ± 1.0 mm of x and y translation at 254.0 µm per revolution, ± 3.2 mm z translation at 318 µm per revolution. The top lens is also placed on a one-axis translation stage (Thorlabs) with a manual actuator which allows 25 mm travel in z-axis with 10 µm resolution. They are finely adjusted so that two beams become confocal and power is maximized. Once the beams are confocal and the feedback intact, the laser is above the threshold, and the signal power is at its maximum with the given current, whereas pump power is at its minimum. A lower cavity loss and a higher stability can be achieved by shortening the optical train.

Then comes the alignment of the illumination. The first step is to set the illimunation light. The LED is easily couples to the multimode fiber in which the end of it is mounted on the breadboard and projected up to the longest possible distance (the ceiling). The fiber mount is also mounted on a one-axis translation stage which allows 25 mm travel in z-axis with 10 µm resolution. After that, the lens with the focal length of 35 mm is mounted on the breadboard on top of the illumination to collimate the light. The focus is adjusted to image the beam to infinity. The beam should have an either Gaussian or uniform distribution to avoid astigmatism in the image plane. The distance between the lens and the fiber mount could be altered to have the desired beam mode. Next step is the deflect the light toward the camera. The mirror at 45° is mounted on a kinematic mounts with three manual actuators which allow $\pm 4^{\circ}$ of pitch and yaw adjustment. It is placed on the breadboard and the center is aligned with the vertical axis of the illumination and horizontal axis of the top DM. The mirror will deflect the light toward the DM from which the light will be deflected toward the cavity. The laser beam and illumination should be confocal before entering and leaving the lenses. The desired propagation of light could be achieved by the degree of freedom the 45° mirror has. The DM's actuators can be utilized, if necessary. Once

the illumination is deflected at the bottom DM, it should be aligned with the camera which is mounted on the optical table. The height of the camera is determined by the height of the center of bottom DM which determines the height of the illumination beam.

3.5. Sample Manipulation

Transparent monodisperse microsphere particles (Microparticles, GmbH) are suspended in water to create the sample solution. A chamber between two microscope slides separated by a thin parafilm layer is prepared. The chamber is filled with the sample solution and then sealed with nail polish. The sample lies on top of the sample holder which is mounted on the three-axis translation stage (Thorlabs) with a manual differential adjustors which allows travel of coarse 4 mm and fine 300 µm with resolution of coarse 500 µm revolution and fine 50 µm per revolution. Four columns hold the translation stage on the optical table to roughly adjust the height for the sample to intersect with the position of the focal spot. The translation stage is used for moving the sample in three dimensions, however, a piezo actuator is recommended for more precise movement with computer control.

3.6. Data Acquisition

To characterize an optical trap, trap stiffness along each direction needs to be determined. In standard optical tweezers, the force applied to the particle by the laser with a harmonic optical potential, can be characterized as follows

$$k_{\mathrm{trap}} = \frac{k_{\mathrm{B}}\, T_{\mathrm{K}}}{\sigma^2} = \kappa_{\mathrm{p}} P, \tag{3.2}$$

where k_{trap} is trap stiffness, σ^2 is the variance of the particle position, κ_p is a proportionality constant that was mentioned in Equation (2.25), and P is the laser power. The power and particle displacement should be measured to characterize the trap. In standard optical tweezers, the laser power is constant. It is independent of the particle position. On the other hand, the power depends on the particle position in intracavity

optical trapping, hence, same method for computing trap stiffness won't be accurate. In intracavity optical tweezers, the trap stiffness needs to be characterized as

$$k_{\text{trap}} = \kappa_{\text{p}} P(r), \tag{3.3}$$

where the power depends on particle position. The nonlinear feedback forces arise when particle position and laser power's are coupled, resulting the non-harmonic trap potential. The power of the laser and trap stiffness depends on particle position as opposed to standard optical tweezers where they are independent of particle position. Hence, in counter-propagating intracavity optical tweezers, simultaneous measurement of both particle displacement and power of two beams is required.

Power measurement of both pump and signal is conducted using photodiode power sensors that are connected to power meters. The power meters are connected to a computer and measurements are monitored simultaneously. The pump power is monitored through the power sensor with infrared (IR) target, which is aligned in the direction of the reflected pump beam from the surface of the top DM. Conversion factor from the measurement at the power sensor to the power on the sample is determined by using reflection and transmission data sheet at the pump wavelength of the DM and the top lens. The signal power is monitored through the port of the inline 50%/50% coupler with the polarization-maintaining fiber coupled to a fiber power sensor. The conversion factor from the measurement at the coupler to the power on the sample is determined by using the loss data sheet of the coupler and the transmission data sheet at the signal wavelength of the DM. The particle's position in the xy-plane is acquired using the custom inverted microscope with the CMOS camera recording at 30 frames per second. The particle's trajectory is measured by digital video microscopy using an open-source MATLAB code [45].

LABVIEW is employed to record simultaneous measurement of powers from the corresponding coupler's port. The graphical programming environment of LABVIEW allows the user to introduce each instrument's driver and control them. The data acquisition rate can be altered. The conversion factor from the power read and the

power on the sample is added. Due to the incompatibility and the lack of driver support of the camera used, only the powermeters were able to be synchronized with LABVIEW. A practical method is employed to overcome this issue. While the data is recorded, the light reaching the camera and signal is blocked at the same time. It marks the time to trim both the video and power data for them to synchronize.

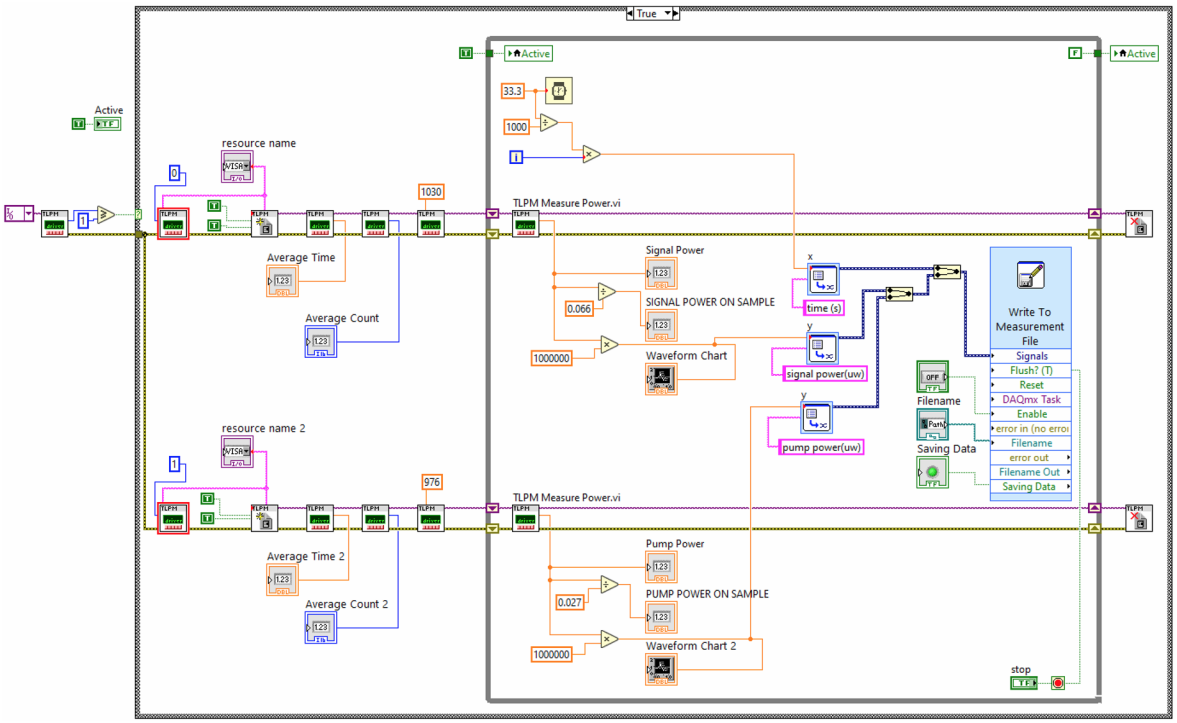

Figure 3.5. The LABVIEW environment for the control of the powermeters.

3.7. Experiment

The trapping experiments are performed on transparent microspheres of silica and polystyrene with various diameters. Power measurement of both pump and signal is recorded when a particle is in the trap. With digital video microscopy, the trapped particle's position is recorded to be tracked and traced later. All measurements are carried out at room temperature.

When the system is aligned, signal power is maximum, whereas pump power is minimum. When the sample is inserted, a power drop in signal is observed due to

refraction and scattering from the microscopic slide The top lens is required to be raised to have the focal spot inside the sample. The translation stage can be utilized to move the sample in the axial direction to focus the image. The signal power is maximized when there is no particle on the focal spot. For calibration, a stationary particle is used to determine the position of the focal spot. When the particle is at the center of the focal spot, the signal power drastically drops due to the optical loss invoked my the particle scattering light out of the cavity. The stationary particle is moved axially and radially to observe how the particle's position affects power. Figure 3.6 shows the change in pump and signal powers when the particle is moved radially from the center of the focal spot. For displacement from the center comparable to the particle size, counter-propagating beams demonstrate inverse linear correlation. It must be noted that this observation is strictly limited to the resolution of the translation stage manual adjustors. A piezo-electric translation stage is required for more accurate conclusion.

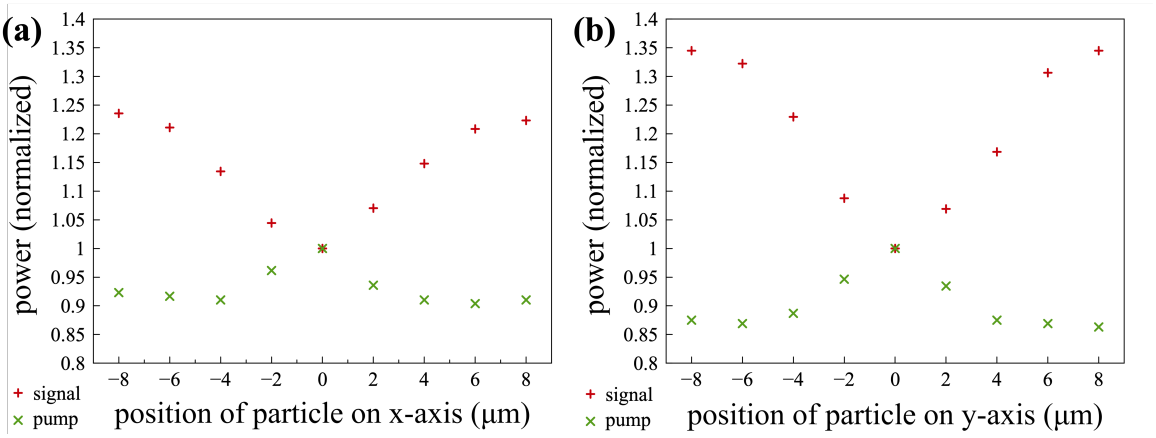

Figure 3.6. A stationary 1.98 µm diameter polystyrene particle is moved (a) in x-axis and (b) in y-axis at the center of the trap. Powers are measured simultaneously and normalized to the power at the center of the focal point [46].

To begin the experiment, the position of the camera should be set and the pixel/length ratio of the image should be determined with a resolution target. It is expected that the equilibrium position of the trapped particle will lie below the focal spot, not at the axial center of it. The camera is positioned to observe focused particles below the focal spot. Figure 3.7 shows the field of view where multiple diffus-

ing particles and a trapped particle are shown. The colours are inverted for a clearer depiction of the image. When the system is ready, the sample is moved in the radial direction to choose a moving particle for trapping. At a distance comparable to the size of the particle, it is possible to observe that the particle is attracted toward the focal spot. When the particle is in the trap, big power fluctuation is observed as the particle moves. As signal power decreases, pump power increases, and vice versa. When the particle is below the focal spot, optical loss of the cavity decreases, which causes the signal power to increase and the particle to be pushed up with scattering force. As the particle approaches the focal point, the optical loss of the cavity increases, which causes the pump power to increase and the particle to be pushed down with scattering force.

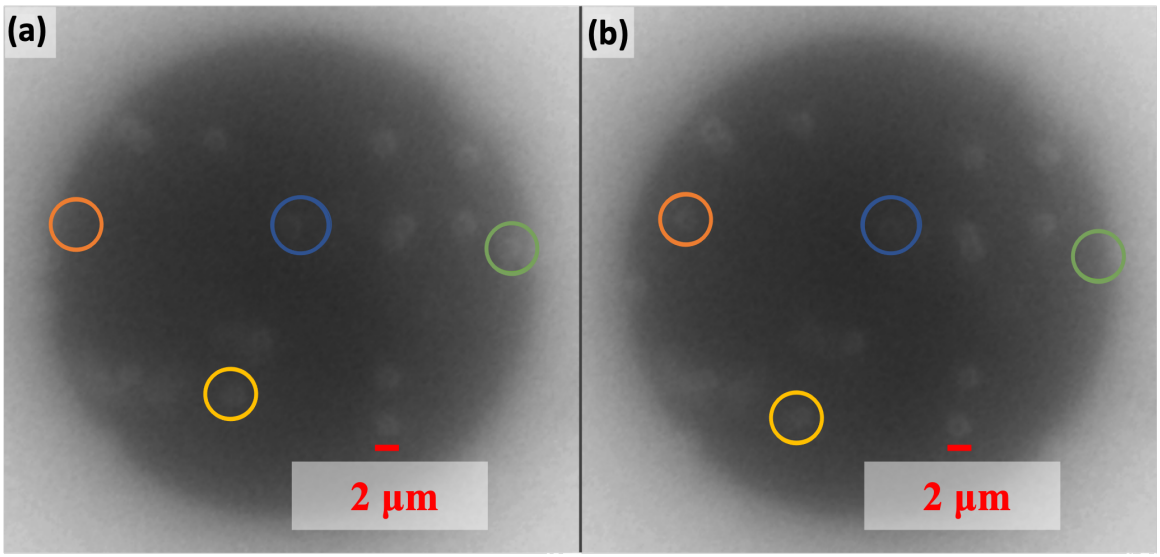

Figure 3.7. The field of view of the camera in two different instants of time (a) and (b) is shown. The trapped particle is shown in the blue circle, while few freely suspended particles are shown in different colors of circles. Note the trajectory of the free particles: they move more than at least twice the particle size whereas the trapped particle is confined in a much smaller area.

Multiple methods can be used to prove 3D trapping. The first method consists in manipulating the particle's axial position in order to prove 3D trapping. When the particle is in the trap, the sample stage is moved down so the trapped particle gets

out of focus. Sometime later, it comes to the focus, meaning, the axial forces pull the particles back to the trap position. Another method exploits the trapping of multiple particles at different depths. When there is a particle in the trap, if another particle at a different depth comes to the trap, 3D trapping of multiple particles should be observed. Moreover, one could also turn the laser off and observe the trapped particle gravitate, and when the laser is turned on again, it should be attracted to the trap. When it is ensured that 3D trapping is achieved and the particle is at the equilibrium position of the trap, the pump and signal power is acquired, and video is recorded at 30 Hz simultaneously.

4. RESULTS

Counter-propagating intracavity optical tweezers demonstrate the ability to trap smaller particles at a lower intensity with an ultra-low NA lens that the other intracavity optial trapping methods was not able to achieve. This Chapter presents and analyses the results of the experiment presented in the previous section.

4.1. Trapping of Polystyrene Particles

Counter-propagating intracavity optical tweezers are capable of 3D trapping of 1.98 µm-diameter polystyrene particles whereas single-beam intracavity cannot trap polystyrene and silica particles smaller than 4.9 µm and 2.8 µm, respectively.

The laser operates at 110 mA with a signal power of 2.1 mW. A strong optical potential is established, attracting a particle toward the focal spot. Figure 4.1 illustrates how the total average power is always self-adjusted. It shows that the particle was below the focal point before it was attracted to the trapping region. When it approaches the trapping region, it is pushed upward by the forward scattering force in the direction of beam propagation. For each axial step the particle takes, it scatters more light, increasing cavity loss, consequently signal decreases, and the pump increases. Then, the particle reaches the equilibrium point, which is expected to be below the focal point, where it oscillates due to thermal fluctuations. During this process, the total average power on the sample is measured to be 885 µW, which corresponds to the average intensity of 21.2 µW µm^{-2}. The maximum total average power is observed during the first few seconds when the particle was pushed. After that, in few seconds it is minimized just before reaching the equilibrium position of the trap, indicating that the trapping mechanism is decreasing the total average intensity on the sample. It is also observed that when the particle is in the equilibrium position of the trap, there is a race between pump and signal powers on which one of them to dominate. Most of the time, it seems they have equal contribution to the total average power. However, there

are some intervals where the signal stays around at its lowest while the pump power dominates. Further investigation of the correlation between two beams is required.

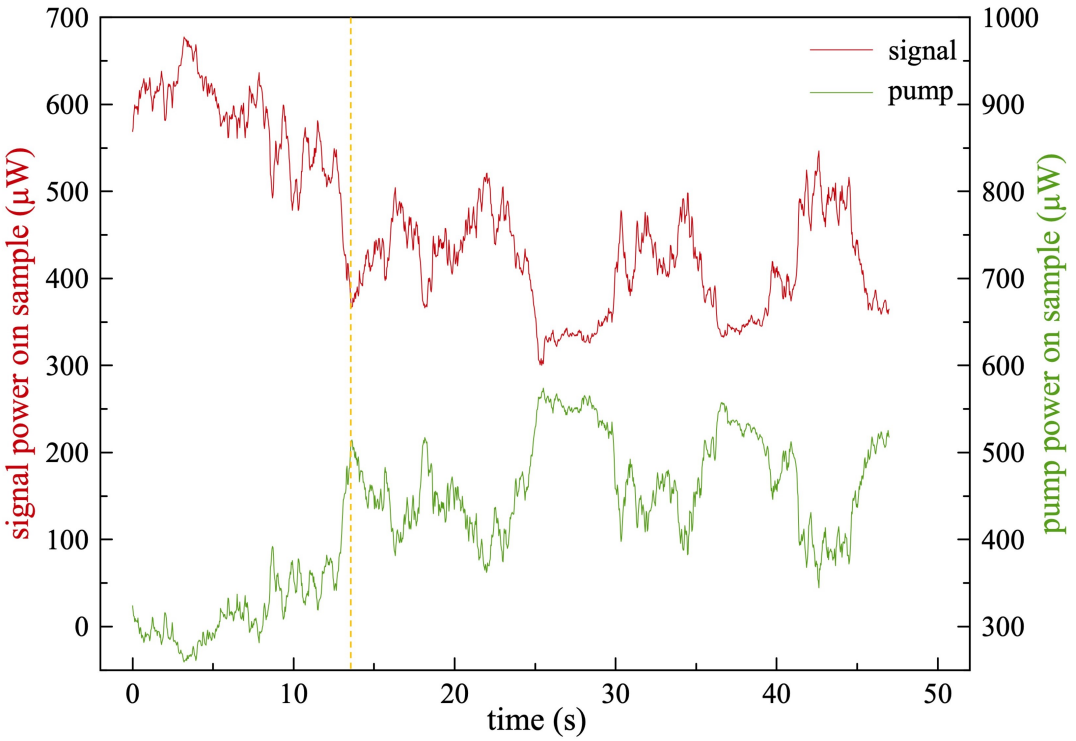

Figure 4.1. Simultaneous measurement of signal and pump power on the sample [46]. The yellow dashed line marks the time when the particle is at the equilibrium position within the trap. The particle is below the focal point, it is pushed to the axial position of the trap, then it oscillates in the equilibrium position within the trap.

4.2. Tracking

The particle tries to escape from the trap due to thermal fluctuations. The coupling between the particle position and the laser power keeps the particle in the trap. When the particle is in the equilibrium position of the trap, a video of the particle is acquired and then used to track its position with MATLAB.

The MATLAB code uses standard digital video microscopy algorithms to detect the pixel position of the particle's center from the image for each video frame and then link all the centers to create the trajectory. The pixel position is used to compute

the actual two-dimensional (2D) position of the particle. Figure 4.2 shows the particle displacement within the trap. The pixel-to-µm ratio of the image is determined with a resolution target. The variance of particle position x and y axis is 0.36 µm^2 and 0.20 µm^2, respectively. The range the particle moves in the x and y axis is 2.91 µm and 2.25 µm, respectively. The median has an offset of 0.45 µm and 0.05 µm with respect to the middle point of the range x and y axis respectively. It can be deduced that the beam centers are slightly misaligned.

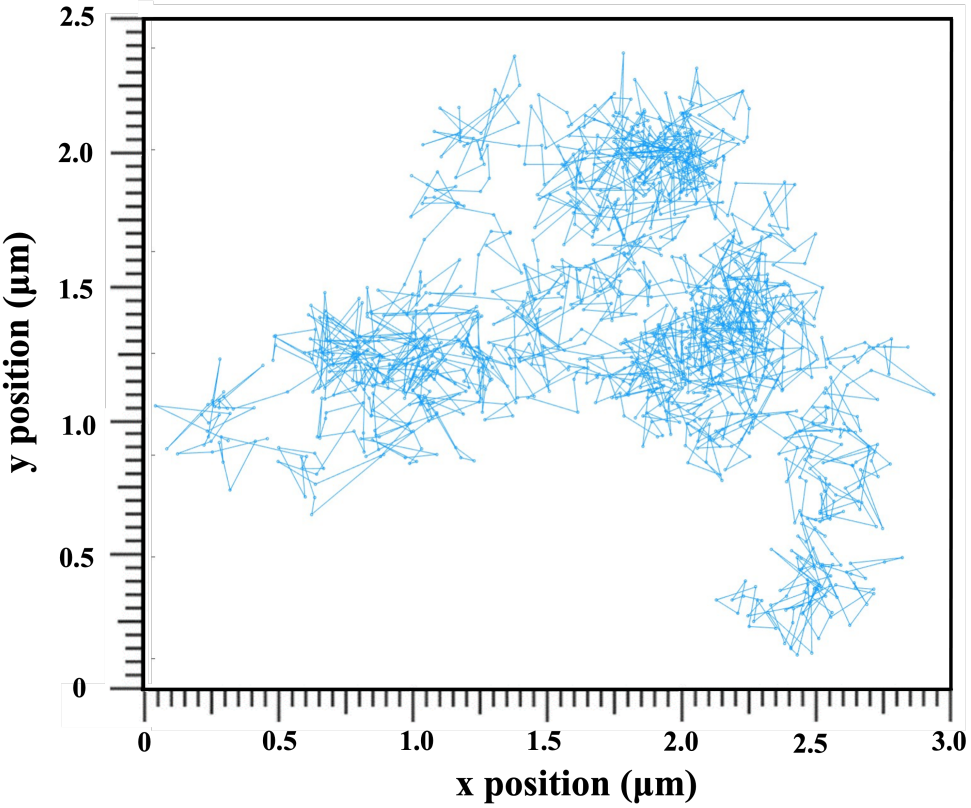

Figure 4.2. The tracking of the particle position in the trap from the recorded video [46]. The pixel position of the particle's center is detected frame by frame and then linked to create the trajectory of the particle within the trap region.

4.3. Comparison of Optical Tweezers

Intracavity optical tweezers demonstrate to trap diameter of 4.9 µm and 6.0 µm diameter polystyrene, and 2.8 µm, 4.0 µm and 4.8 µm um diameter silica particles. It is capable of 3D trapping single yeast cells, typically around 4 µm in diameter,

with an average power of 0.47 mm, corresponding to an intensity of 0.036 mW µm^{-2} However, it cannot trap smaller particles whereas the counter-propagating intracavity optical tweezers are capable of 3D trapping of 1.98 µm polystyrene particle with total average power on the sample of 885 µW, which corresponds to the average intensity of 21.2 µW µm^{-2}. The variance of particle position x-axis is 0.36 µm^2, in the y-axis is 0.20 µm^2. Figure 4.3 compares the radial trapping efficiency versus diameter of the findings of this thesis with single-beam intracavity optical tweezers and standard high NA optical tweezers. Counter-propagating configuration of intracavity optical tweezers allows for trapping of smaller particles; however, the same level of efficiency that the single-beam configuration has with trapping of larger particles is not established.

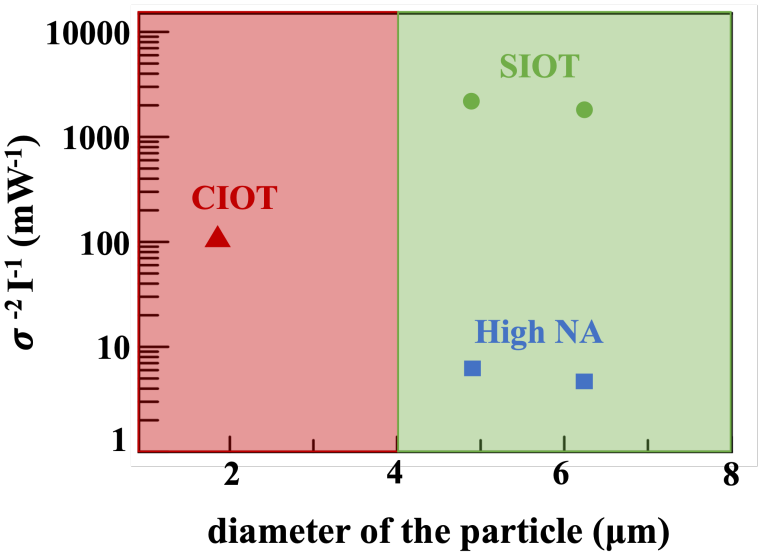

Figure 4.3. The radial trapping efficiency of trapping polystyrene particles versus the diameter. Comparison among CIOT, SIOT, and standard high NA optical tweezers. The red triangle marks the result of the experiment that is presented in this thesis. Green circle and blue squares marks the results from [11]. CIOT are able to trap the particles that the SIOT fail to trap.

4.4. Limitations of Counter-Propagating Intracavity Optical Tweezers

The counter-propagating intracavity optical tweezers presented in this thesis can 3D trapping polystyrene particles as small as 1.98 µm at average power as low as

486 µW. However, the inverted microscope only allows for imaging in the xy-plane, thus, tracking of particle position in three dimensions is not feasible with conventional methods.

Three-dimensional trapping requires extremely sensitive alignment of the two beams with a spot size of 7.1 µm and 7.5 µm. The precision of the alignment relies on the optomechanical components with manual adjusters. The relatively low resolution given by the adjusters (knurled knobs) with respect to the spot size introduces some inevitable human error. When the system is slightly misaligned in the xy-plane, the particle is likely to escape from the trap. On the other hand, when the system is slightly misaligned along the z-axis, 3D trapping is still feasible. However, the trap stiffness weakens, and the particle's motion along the z-axis increases. Consequently, the depth of field becomes inadequate for accurate 2D tracking of the trapped particle. The ability of the tracking also depends on the quality of the image. The quality of the image affects the ability to characterize the feedback forces. For the digital video microscopy algorithm to detect the center of the particle, the image needs sufficient intensity and contrast. Utilizing trapping effectively depends on the capabilities of imaging.

5. CONCLUSION

To conclude, this thesis aimed to examine intracavity optical trapping techniques and provide new findings with counter-propagating intracavity optical tweezers. Through detailed experimentation, data analysis, and critical evaluation, the research objectives have been successfully achieved.

5.1. Findings

This work demonstrated 3D trapping of 1.98 µm diameter polystyrene with self-adjusted counter-propagating intracavity optical tweezers. While simply trapping small polystyrene particles sounds straightforward, the experiments are laborious. The beam alignment procedure possesses many challenges that reveal the system's extreme sensitivity. The stability of the feedback forces heavily relies on the precise alignment of the two beams. Once the precise alignment is achieved, the feedback mechanism reveals itself. The laser power is self-regulated by the particle's displacement. The two beams are inversely correlated, yet a realizable correlation coefficient does not appear. On the other hand, using ultra-low NA lenses dramatically reduces the laser intensity on the trapped particle as opposed to standard optical tweezers.

Using counter-propagating beams cancels the dominating scattering force; thus, the trapping strength increases, which allows for trapping smaller particles. This configuration results in more confinement per NA than other intracavity and standard optical tweezers. Experimentally it has been realized that the position of the particle can be manipulated radially and axially to separate a single trapped participle from surrounding freely suspended particles. It has been observed that the trapping of multiple particles at once is possible, however, all particles don't experience the same restoring force. One can separate a single particle from the group by moving the sample plane quickly. The particle outside the center cannot stay in the trap at a reasonable speed. Due to low average power, counter-propagating intracavity optical tweezers can

trap particles over long periods without risk of photodamage. Note that the temperature plays a significant role to observe trapping. If experiments are performed below room temperature, the optical potential is not enough to attract or push a gravitated particle.

5.2. Contribution and Significance

The 3D trapping of 1.98 µm polystyrene bead at a total average power of 885 µW have shed light on further capabilities of intracavity optical tweezers and contributed to the existing body of knowledge. It promises application on the biological matter subjected to photodamage due to laser light intensity.

Several key insights have emerged throughout the experimentation process, revealing the complexities and limitations of the proposed optical setup. Information about the system's design, implementation, and development is improved. The findings have led to academic publications [46,47] and opened new opportunities for further improvement of intracavity optical tweezers.

5.3. Future Work

This work analyzes two optical configurations for intracavity optical trapping: a forward pumping configuration and a backward pumping configuration. It exploits the capabilities of optical trapping by counter-propagating beams within the laser cavity with a backward pumping configuration.

The feedback mechanism in the forward pumping configuration has been identified and confirmed. However, a consistent and predictable correlation between the counter-propagating beams in the backward pumping configuration and the particle's displacement remains elusive. There may be additional factors involved that have not yet been accounted for. The toy model in the forward pumping configuration needs to be extended to the counter-propagating intracavity optical tweezers. Further research

and investigations are needed to identify any pattern or relationship between the power of the beams and the particle displacement to characterize the system.

A similar system with different laser parameters is also established. It is built with a similar fiber-coupled diode laser to create a CW ring cavity laser, but with all non-polarization-maintaining fiber operating at 1030 nm. It uses a segment of Yb-doped fiber as gain and employs an inline isolator. It is able to use an ultra-low NA (about 0.09) lens for trapping. The 3D trapping of 1.98 µm diameter polystyrene is achieved as well with a total average power of 486 µW on the sample, which corresponds to an average intensity of 11.6 µW µm^{-2}. However, the image quality does not allow for tracking. At the given total average power, axial trap stiffness decreases dramatically. The particle movement lies outside the depth of field which the tracking algorithm can detect.

It is necessary to improve the imaging system to investigate further the capabilities of optical trapping facilitated by CIOT. Two different imaging modalities have been developed with the counter-propagating intracavity optical tweezers: Holography-assisted-intracavity optical tweezer, and real-time 3D tracking of a microparticle using chromatic aberration.

Integrating holographic microscopy with optical tweezers has already been proposed and shown promising results to track the position of the trapped particle. It was logical to combine it with the counter-propagating intracavity optical tweezers as well. Mach-Zehner holography method has been employed with a He-Ne laser. Two set of experiment with 8 mm and 11 mm aspheric lenses has been performed. Without the trapping mechanism at play, the topography of red blood cells has been reconstructed yet it was inconclusive. As for future work, optimizing the setup is needed to establish the axial position of the particle.

A more efficient way to tracking of microparticles can be exploited. Using chromatic aberration, real-time 3D tracking of a microparticle has been investigated [48].

Chromatic aberration of the lens allows to take advantage of the focal length variation with the wavelength. When the axial movement of the particle is mapped to lateral movements in the image plane, computation of the 3D coordinates of the particle becomes possible. This method allows us to investigate the position of a 6.24 µm polystyrene particle suspended in water with an error lower than 1 µm. It is able to make predictions at a rate of 1.5 kHz. As for future work, this method can be extended to sub-micron particle tracking and can be integrated with any optical tweezers setup to offer a great alternative to other tracking methods such as digital holography.

In conclusion, this work has laid the foundations for extending capabilities offered by intracavity optical tweezers with counter-propagating beams within the laser cavity, and it has inspired the author's future research on laser-matter interactions within biomedical applications.

REFERENCES

1. He, X., K. Wang, J. Zhuang, P. Xu, X. Gao, R. Guo, C. Sheng, M. Liu, J. Wang, J. Li, G. V. Shlyapnikov and M. Zhan, "Coherently Forming a Single Molecule in an Optical Trap", *Science*, Vol. 370, No. 6514, pp. 331–335, 2020.

2. Barak, P., A. Rai, P. Rai and R. Mallik, "Quantitative Optical Trapping on Single Organelles in Cell Extract", *Nature Methods*, Vol. 10, No. 1, pp. 68–70, 2013.

3. Pang, Y. and R. Gordon, "Optical Trapping of a Single Protein", *Nano Letters*, Vol. 12, No. 1, pp. 402–406, 2012.

4. Nawaz, S., P. Sánchez, K. Bodensiek, S. Li, M. Simons and I. A. Schaap, "Cell Visco-Elasticity Measured with AFM and Optical Trapping at Sub-Micrometer Deformations", *PLoS One*, Vol. 7, No. 9, pp. 1–9, 2012.

5. Ashkin, A., "Acceleration and Trapping of Particles by Radiation Pressure", *Physical Review Letters*, Vol. 24, No. 4, pp. 156–159, 1970.

6. Chu, S., J. Bjorkholm, A. Ashkin and A. Cable, "Experimental Observation of Optically Trapped Atoms", *Physical Review Letters*, Vol. 57, No. 3, pp. 314–317, 1986.

7. Ashkin, A. and J. M. Dziedzic, "Optical Trapping and Manipulation of Viruses and Bacteria", *Science*, Vol. 235, No. 4795, pp. 1517–1520, 1987.

8. Ashkin, A., K. Schütze, J. Dziedzic, U. Euteneuer and M. Schliwa, "Force Generation of Organelle Transport Measured in Vivo by an Infrared Laser Trap", *Nature*, Vol. 348, No. 6299, pp. 346–348, 1990.

9. Tuna, Y., R. Sayed, M. G. Donato, P. G. Gucciardi, O. M. Maragò and G. Volpe, "Optical Feedback Radiation Forces: Intracavity Optical Trapping with Feedback-

locked Diode Lasers", *Frontiers in Optics 2012/Laser Science XXVIII*, Rochester, USA, pp. 1–2, 2012.

10. Sayed, R., F. Kalantarifard, P. Elahi, F. O. Ilday, G. Volpe and O. M. Maragò, "Intracavity Optical Trapping with Ytterbium Doped Fiber Ring Laser", *Optical Trapping and Optical Micromanipulation X*, edited by Dholakia K. and G.C Spalding, San Diego, USA, Vol. 8810, pp. 364–371, 2013.

11. Kalantarifard, F., P. Elahi, G. Makey, O. M. Maragò, F. Ö. Ilday and G. Volpe, "Intracavity Optical Trapping of Microscopic Particles in a Ring-Cavity Fiber Laser", *Nature Communications*, Vol. 10, No. 1, pp. 1–11, 2019.

12. Lebedew, P., "Untersuchungen über die Druckkräfte des Lichtes", *Annalen der Physik*, Vol. 311, No. 11, pp. 433–458, 1901.

13. Nichols, E. F. and G. F. Hull, "The Pressure Due to Radiation", *Proceedings of the American Academy of Arts and Sciences*, Vol. 38, No. 20, pp. 559–599, 1903.

14. Einstein, A., "Zur Quantentheorie der Strahlung", *Physikalische Zeitschrift*, Vol. 18, No. 1, pp. 121–128, 1917.

15. Nelson, D. F., R. J. Collins and W. Kaiser, "Bell Labs and the Ruby Laser", *Physics Today*, Vol. 63, No. 1, pp. 40–45, 2010.

16. Thyagarajan, K. and A. Ghatak, *Lasers: Fundamentals and Applications*, Fourth Edition, Springer Science & Business Media, New York, 2010.

17. Maiman, T. H., "Stimulated Optical Radiation in Ruby", *Nature*, Vol. 187, No. 4736, pp. 493–494, 1960.

18. Sorokin, P. P. and M. J. Stevenson, "Stimulated Infrared Emission from Trivalent Uranium", *Physical Review Letters*, Vol. 5, No. 12, pp. 557–559, 1960.

19. Snitzer, E., "Optical Dielectric Waveguides", *PGMTT National Symposium Digest*, Vol. 61, Washington, USA, pp. 45–46, 1961.

20. Koester, C. J. and E. Snitzer, "Amplification in a Fiber Laser", *Applied Optics*, Vol. 3, No. 10, pp. 1182–1186, 1964.

21. Ashkin, A. and J. M. Dziedzic, "Optical Levitation by Radiation Pressure", *Applied Physics Letters*, Vol. 19, No. 8, pp. 283–285, 1971.

22. Ashkin, A., "Trapping of Atoms by Resonance Radiation Pressure", *Physical Review letters*, Vol. 40, No. 12, pp. 729–732, 1978.

23. Ashkin, A., J. M. Dziedzic, J. E. Bjorkholm and S. Chu, "Observation of a Single-Beam Gradient Force Optical Trap for Dielectric Particles", *Optics Letters*, Vol. 11, No. 5, pp. 288–290, 1986.

24. Chu, S., "Nobel Lecture: The Manipulation of Neutral Particles", *Reviews of Modern Physics*, Vol. 70, No. 3, pp. 685–706, 1998.

25. Neuman, K. C., E. H. Chadd, G. F. Liou, K. Bergman and S. M. Block, "Characterization of Photodamage to Escherichia Coli in Optical Traps", *Biophysical Journal*, Vol. 77, No. 5, pp. 2856–2863, 1999.

26. Dutra, R. S., N. B. Viana, P. A. M. Neto and H. M. Nussenzveig, "Polarization Effects in Optical Tweezers", *Journal of Optics A: Pure and Applied Optics*, Vol. 9, No. 8, pp. S221–S227, 2007.

27. Rubinsztein-Dunlop, H., T. Nieminen, M. Friese and N. Heckenberg, "Optical Trapping of Absorbing Particles", *Advances in Quantum Chemistry*, Vol. 30, No. 1, pp. 469–492, 1998.

28. Pacoret, C., R. Bowman, G. Gibson, S. Haliyo, D. Carberry, A. Bergander, S. Régnier and M. Padgett, "Touching the Microworld with Force-Feedback Optical

Tweezers", *Optics Express*, Vol. 17, No. 12, pp. 10259–10264, 2009.

29. Liang, H., W. H. Wright, S. Cheng, W. He and M. W. Berns, "Micromanipulation of Chromosomes in PTK2 Cells Using Laser Microsurgery (Optical Scalpel) in Combination with Laser-Induced Optical Force (Optical Tweezers)", *Experimental Cell Research*, Vol. 204, No. 1, pp. 110–120, 1993.

30. Keloth, A., O. Anderson, D. Risbridger and L. Paterson, "Single Cell Isolation Using Optical Tweezers", *Micromachines*, Vol. 9, No. 9, 2018.

31. Ashkin, A. and J. M. Dziedzic, "Internal Cell Manipulation Using Infrared Laser Traps", *Proceedings of the National Academy of Sciences of the United States of America*, Vol. 86, No. 20, pp. 7914–7918, 1989.

32. Block, S. M., L. S. Goldstein and B. J. Schnapp, "Bead Movement by Single Kinesin Molecules Studied with Optical Tweezers", *Nature*, Vol. 348, No. 6299, pp. 348–352, 1990.

33. Perkins, T. T., S. R. Quake, D. E. Smith and S. Chu, "Relaxation of a Single DNA Molecule Observed by Optical Microscopy", *Science*, Vol. 264, No. 5160, pp. 822–826, 1994.

34. Mourou, G., "Nobel Lecture: Extreme Light Physics and Application", *Reviews of Modern Physics*, Vol. 91, No. 3, pp. 1–21, 2019.

35. Shen, Y. C. and G. D. Lin, "Scalable Quantum Computing Stabilised by Optical Tweezers on an Ion Crystal", *New Journal of Physics*, Vol. 22, No. 5, pp. 1–12, 2020.

36. Alali, H., Z. Gong, G. Videen, Y.-L. Pan, O. Muñoz and C. Wang, "Laser Spectroscopic Characterization of Single Extraterrestrial Dust Particles Using Optical Trapping-Cavity Ringdown and Raman Spectroscopy", *Journal of Quantitative Spectroscopy and Radiative Transfer*, Vol. 255, No. 107249, pp. 1–8, 2020.

37. Yuan, S., Q. Zheng, B. Yao, M. Wen, W. Zhang, J. Yuan and H. Lei, "Bio-Compatible Miniature Viscosity Sensor Based on Optical Tweezers", *Biomediacal Optics Express*, Vol. 13, No. 3, pp. 1152–1160, 2022.

38. Jones, P. H., O. M. Maragò and G. Volpe, *Optical Tweezers: Principles and Applications*, Cambridge University Press, Cambridge, 2015.

39. Ashkin, A., "Forces of a Single-Beam Gradient Laser Trap on a Dielectric Sphere in the Ray Optics Regime", *Biophysical Journal*, Vol. 61, No. 2, pp. 569–582, 1992.

40. Yang, Y., Y. Ren, M. Chen, Y. Arita and C. Rosales-Guzmán, "Optical Trapping with Structured Light: A Review", *Advanced Photonics*, Vol. 3, No. 3, pp. 1–40, 2021.

41. Pitzek, M., R. Steiger, G. Thalhammer, S. Bernet and M. Ritsch-Marte, "Optical Mirror Trap with a Large Field of View", *Optics Express*, Vol. 17, No. 22, pp. 19414–19423, 2009.

42. Ashkin, A., "History of Optical Trapping and Manipulation of Small-Neutral Particle, Atoms, and Molecules", *IEEE Journal of Selected Topics in Quantum Electronics*, Vol. 6, No. 6, pp. 841–856, 2000.

43. Paul, M. C., *Fiber Laser*, IntechOpen, London, 2016.

44. Jackson, S., R. Vallee and M. Bernier, *"Mid-Infrared Fiber Photonics: Glass Materials, Fiber Fabrication and Processing, Laser and Nonlinear Sources"*, Woodhead Publishing, Sawston, 2021.

45. Callegari, A., M. Mijalkov, A. B. Gököz and G. Volpe, "Computational Toolbox for Optical Tweezers in Geometrical Optics", *Journal of the Optical Society of America B*, Vol. 32, No. 5, pp. B11–B19, 2015.

46. Ay, A. and P. Elahi, "Ultra-Low Numerical Aperture Counter-Propagating Intra-

cavity Optical Tweezers", *Specialty Optical Fibres*, edited by Kalli K., A. Mendez and P. Peterka, Vol. 12573, Prague, Czech Republic, pp. 1–5, 2023.

47. Ciarlo, A., G. Pesce, F. Kalantarifard, P. Elahi, G. Volpe and A. Sasso, "Intracavity Feedback Optical Trapping", *Il Nuovo Cimento C*, Vol. 45, No. 6, pp. 1–4, 2022.

48. Elahi, S., A. Ay and P. Elahi, "Real-time 3D tracking of a microparticle using chromatic aberration", *Real-time Processing of Image, Depth and Video Information 2023*, edited by Carlsohn, M. K., Vol. 12571, Prague, Czech Republic, pp. 1–8, 2023.